Concepts in Imaging and Microscopy

Imaging Membrane Potential With Voltage-Sensitive Dyes

MICHAL ZOCHOWSKI,[1,*] MATT WACHOWIAK,[1] CHUN X. FALK,[2] LAWRENCE B. COHEN,[1,2] YING-WAN LAM,[1] SRDJAN ANTIC,[1] AND DEJAN ZECEVIC[1]

[1] *Department of Cellular and Molecular Physiology, Yale University School of Medicine New Haven, Connecticut 06520; and* [2] *RedShirtImaging, LLC, Fairfield, Connecticut 06432*

Abstract. Membrane potential can be measured optically using a variety of molecular probes. These measurements can be useful in studying function at the level of an individual cell, for determining how groups of neurons generate a behavior, and for studying the correlated behavior of populations of neurons. Examples of the three kinds of measurements are presented. The signals obtained from these measurements are generally small. Methodological considerations necessary to optimize the resulting signal-to-noise ratio are discussed.

Introduction

An optical measurement of membrane potential using a molecular probe can be beneficial in a variety of circumstances. One advantage is the ability to measure from many locations simultaneously. This is especially important in the study of nervous systems in which many parts of an individual cell, or many cells, or many regions of the nervous system are active at the same time. In addition, optical recording offers the possibility of recording from processes that are too small or fragile for electrode recording.

Several optical properties of membrane-bound dyes are sensitive to membrane potential, including fluorescence, absorption, dichroism, birefringence, fluorescence resonance energy transfer, nonlinear second harmonic generation, and resonance Raman absorption. However, because the vast majority of applications have involved fluorescence or absorption, these will be emphasized in this review. All of the optical signals described here are "fast" signals (Cohen and Salzberg, 1978) that are presumed to arise from membrane-bound dye; they follow changes in membrane

potential with time courses that are rapid compared to the rise time of an action potential.

Studies of the molecular mechanisms that result in potential-dependent optical properties have produced evidence supporting three mechanisms (for different dyes): dipole rotation, electrochromism, and a potential-sensitive monomer-dimer equilibrium. Dye mechanisms are discussed in Waggoner and Grinvald (1977), Loew *et al.* (1985), and Fromherz *et al.* (1991).
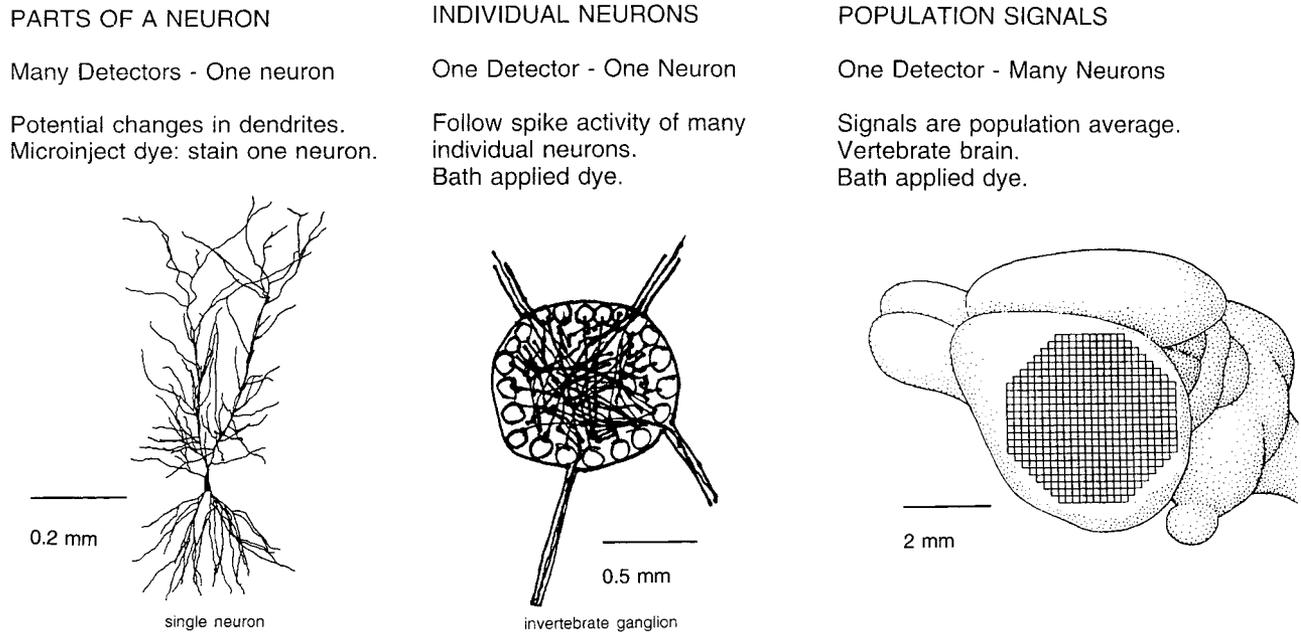
We begin with examples of results obtained from measurements addressing three quite different neurobiological problems. In all three instances the camera was a photodiode array with only 464 pixels (NeuroPlex; RedShirtImaging, LLC, Fairfield, CT). Despite this low spatial resolution, the camera resolution was not limiting in any of the examples. On the positive side, this camera has an outstanding dynamic range; with an incident intensity of more than 10^{10} photons per frame, it measures signals that are a fractional change ($\Delta I/I$) of one part in 10^5. In addition, it has a frame rate of 1.6 kHz (fast enough to measure most neurobiologically important signals). On the other hand, recently introduced CCD cameras not only have similar frame rates but also have lower dark noise. Thus, in one of the three measurements, we think that improved signal-to-noise ratios could be obtained with a cooled CCD camera. The optical signals in the example measurements are not large—they represent fractional changes in light intensity ($\Delta I/I$) of from 10^{-4} to 3×10^{-2}. Nonetheless, they can be measured with an acceptable signal-to-noise ratio after attention to details of the measurement that are described in the second part of the paper.

Figure 1 illustrates three qualitatively different areas of neurobiology in which imaging membrane potential has been useful. First (left panel), to know how a neuron integrates its synaptic input into its action potential output, one must be able to measure membrane potential wherever synaptic input occurs and at the places where spikes are initiated. Second (middle panel), to understand how a nervous system generates a behavior, the action potential activity of many (all) of the participating neurons must be

PARTS OF A NEURON

Many Detectors - One neuron

Potential changes in dendrites.
Microinject dye: stain one neuron.

INDIVIDUAL NEURONS

One Detector - One Neuron

Follow spike activity of many
individual neurons.
Bath applied dye.

POPULATION SIGNALS

One Detector - Many Neurons

Signals are population average.
Vertebrate brain.
Bath applied dye.

0.2 mm

single neuron

0.5 mm

invertebrate ganglion

2 mm

Figure 1.   Schematic of the three kinds of measurements described as examples. (Left) An individual cortical hippocampal CA1 pyramidal cell. Each pixel of the 464-element photodiode array receives light from a small part of the dendrite, axon, or cell body of the neuron. An optical measurement of membrane potential provides information about how the neuron converts its synaptic input into its spike output. (Middle) A slice through an invertebrate ganglion with its cell bodies in a cortex around the outside and neuropil in the middle. Here each detector receives light from one or a small number of cell bodies. A voltage-sensitive dye measurement of spike activity while the ganglion is generating a behavior provides information about how the behavior is generated. (Right) A vertebrate brain with the superimposed 464-element photodiode array (used in all three examples). Each pixel of the array receives light from thousands of cells and processes. The signal is the population average of the change in membrane potential in those cells and processes. The image of the hippocampal neuron was taken from Mainen *et al.* (1996).

measured simultaneously. Third (right panel), responses to sensory stimuli and generation of motor output in the vertebrate brain are often accompanied by synchronous activation of many neurons in widespread brain areas; voltage-sensitive dye recordings allow simultaneous measurement of population signals from many areas. In these three instances, optical recordings have provided kinds of information about the function of the nervous system that were previously unobtainable.

In the second half of the article, we describe the experimental details that are important in obtaining the signal-to-noise ratios achieved in the experiments described in the first section. We discuss signal type, dyes, light sources, photodetectors, and optics.

Three Examples

1. Processes of an individual neuron (Fig. 1, left panel)

Understanding the biophysical properties of single neurons and how they process information is fundamental to understanding how the brain works. With the development of new measuring techniques that allow more direct inves-

tigation of individual nerve cells, it became widely recognized, especially during the last 20 years, that dendritic membranes of many vertebrate CNS neurons contain active conductances such as voltage-activated Na^+, Ca^{2+}, and K^+ channels (*e.g.,* Stuart and Sakmann, 1994; Spruston *et al.,* 1995; Magee and Johnston, 1995; Magee *et al.,* 1995). An important consequence of active dendrites is that regional electrical properties of branching neuronal processes will be extraordinarily complex, dynamic, and, in the general case, impossible to predict in the absence of detailed measurements.

To obtain such a measurement one would, ideally, like to monitor, at multiple sites, subthreshold events as they travel from the sites of origin on neuronal processes and summate at particular locations to influence the initiation of action potentials. This goal has not been achieved in any neuron, vertebrate or invertebrate, due to the technical limitations of measurements that employ electrodes. Better spatial resolution necessitates a turn from direct electrical recording to indirect, optical measurements using voltage-sensitive dyes. Recently, the sensitivity of intracellular voltage-sensitive dye techniques for monitoring neuronal processes *in situ* has
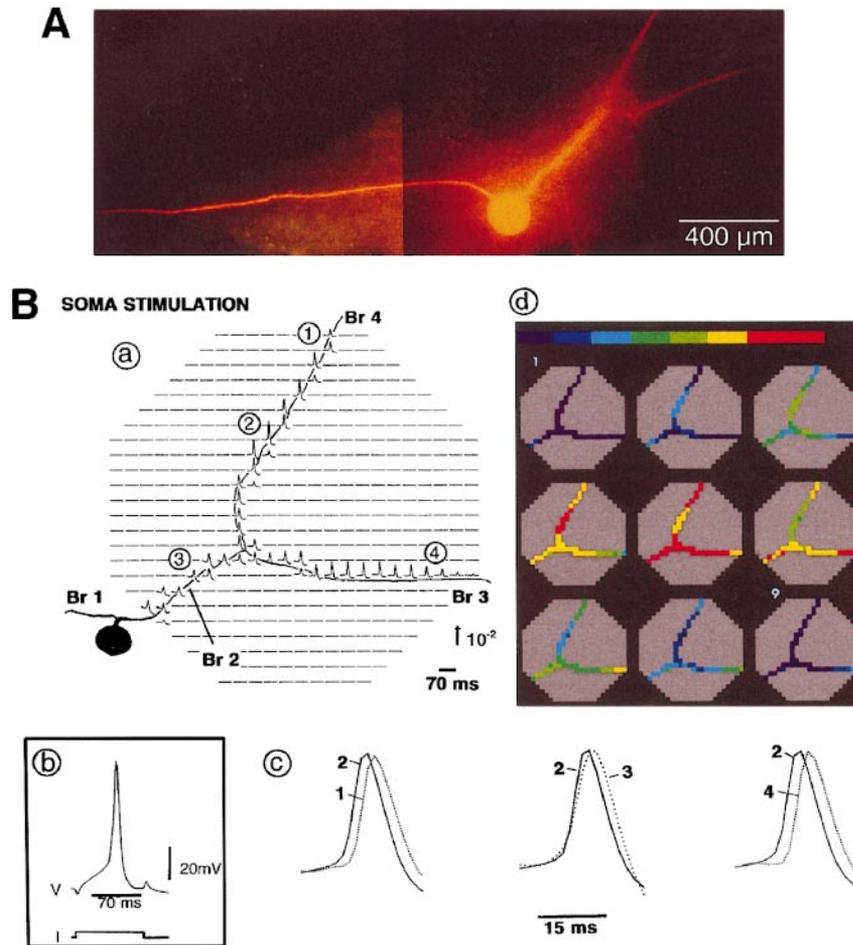
Figure 2. (A) Giant metacerebral neuron from the left cerebral ganglion 12 h after injection with the fluorescent voltage-sensitive dye JPW1114. The cell body and main processes are clearly visible in the unfixed preparation. Excitation wavelength: 540 ± 30 nm; dichroic mirror: 570 nm, long-pass barrier filter: 610 nm. (B) (Ba) Voltage-sensitive dye recording of action potential signals from elements of the photodiode array positioned over the image of axonal arborizations of a metacerebral cell in the left cerebral ganglion. Axonal branches are marked Br 1–4. Spikes were evoked by transmembrane current steps, as shown in (Bb), delivered through the recording microelectrode in the soma. Each optical trace in (Ba) represents 70 ms of recording centered around the peak of the spike as indicated by the time bar in (Bb). Each diode received light from a 50×50 μm area in the object plane. (Bc) Recordings from four locations indicated in panel (Ba), scaled to the same height, are compared to determine the site of the origin of the action potential and the direction of propagation. (Bd) Color-coded representation of the data shown in (Ba) indicating the size and location of the primary spike-trigger zone and the pattern of spike propagation. Consecutive frames represent data points that are 1.6 ms apart. The color scale is relative, with the peak of the action potential for each detector shown in red (modified from Zecevic, 1996).

been improved by a factor of roughly 150, allowing direct recording of subthreshold and action potential signals from the neurites of invertebrate neurons (Antic and Zecevic, 1995; Zecevic, 1996). The improvement in the signal-to-noise ratio is based on previous experience from other laboratories (Davila *et al.,* 1974; Grinvald *et al.,* 1987) and on (1) finding an intracellular dye that provides a relatively large fractional change in fluorescence and (2) improvements in the apparatus to increase the incident light inten-

sity, to lower the noise, and to filter more efficiently. Encouraging results have also been obtained in initial studies on vertebrate CNS neurons in brain slices (see below).

An invertebrate neuron. A typical result of a multi-site voltage-sensitive dye recording is shown in Figure 2. The fluorescent image of a metacerebral *Helix* neuron following injection with the fluorescent voltage-sensitive dye JPW1114 is shown in Figure 2A. The image of the cell was projected onto the array of photodiodes as indicated in

Figure 2Ba. This panel represents multi-site recording of action-potential signals from axonal branches Br2, Br3, and Br4, evoked by a transmembrane current step (Fig. 2Bb). Optical signals associated with action potentials, expressed as fractional changes in fluorescent light intensity ($\Delta F/F$), were between 3×10^{-3} and 3×10^{-2} in recordings from the processes. With these measurements it is straightforward to determine the direction and velocity of action-potential propagation in neuronal processes. In Figure 2Bc, recordings from different locations, scaled to the same height, are compared to determine the site of origin of the action potential. The earliest action potential, in response to soma stimulation, was generated near location 2, in the axonal branch Br4, situated in the cerebral-buccal connective outside the ganglion. The spike propagated orthodromically from the site of initiation toward the periphery in branch Br4 and antidromically toward the soma and into the branch Br3 in the external lip nerve. The direction of propagation is clear from the color-coded representation of the data (Fig. 2Bd). This figure shows the potential changes in the branching structure at nine different times separated by 1.6 ms. Red corresponds to the peak of the action potential. The panels show the position of the action-potential trigger zone at location 2 and orthodromic and antidromic spread of the nerve impulse from the site of initiation. The earliest spike was evoked about 1 mm from the soma. The spike-initiation segment in the axon is roughly 300 μm in length and remote from the soma. It appears that under normal conditions, slow depolarizing voltage pulses applied to the soma are electrotonically spread into the processes with little attenuation. These depolarizing pulses initiate action potentials in the processes at remote sites that are more excitable than neighboring segments.

Light scattering in the ganglion limits the maximum useful spatial resolution in this kind of measurement. Thus the 24×24 pixel resolution of NeuroPlex appears to be adequate in this circumstance.

On the basis of similar measurements, we recently determined that the *Helix* neuron in Figure 2 has multiple trigger zones that can be independently activated. The precise pattern of action-potential initiation and propagation within the whole branching structure of a neuron can be analyzed by multi-site recording. The information about the spatial and temporal dynamics of neuronal signals can be used to constrain the choice of channel densities and geometrical factors in biophysical models that are used to describe functional properties of neurons.

A vertebrate neuron. It is of considerable interest to apply the same technique to dendrites of vertebrate CNS neurons in brain slices. Apart from our preliminary experiments (Kogan *et al.,* 1995), there is no previous experience in this field. Experiments were carried out on pyramidal neurons in slices from the neocortex of 14- to 18-day-old rats. The fluorescent image of the cell was projected onto the octag-

onal photodiode array. In the example shown in Figure 3A, the neuron was stimulated, by depolarizing the cell body, to produce a burst of two action potentials. Each trace in Figure 3B represents the output of one photodiode for 44 ms. Optical signals associated with action potentials, expressed as fractional changes in fluorescent light intensity ($\Delta F/F$), were between 10^{-2} and 3×10^{-2} in recordings from the processes. In Figure 3C, the electrical recordings from the soma (smooth line) were compared with the optical signals filtered to eliminate high-frequency noise (dashed line). The time courses of electrical and optical recordings agree well. In panel D, recordings from different locations, scaled to the same height, are compared on an expanded time scale. Each trace is a spatial average from two adjacent detectors. Both spikes in the burst originated near the soma and propagated centrifugally along the apical and basolateral dendrites (action potential back-propagation; Stuart and Sakmann, 1994).

These initial experiments demonstrate several important methodological results. First, it is possible to deposit the dye into the cell without staining the surrounding tissue (keeping background fluorescence low). Second, the pharmacological effects of the dye were completely reversible if the staining pipette was withdrawn, and the cell was allowed to recover for 1–2 h. Third, the level of photodynamic damage already allows meaningful measurements and could be reduced further. Finally, the sensitivity of the dye was comparable to that achieved in the experiments on invertebrate neurons (Zecevic, 1996). In these preliminary experiments, the dye spread for roughly 500 μm into dendritic processes within 2 h. One way to improve the staining is to attach the dye electrode to the distal region on a dendrite as done previously with calcium-sensitive dyes (*e.g.,* Markram and Sakmann, 1994; Schiller *et al.,* 1995). This approach will shorten the time needed for diffusion.

The light intensity at the photodetector in the measurements from the distal process of these neurons is low; the dark noise of the 464-element photodiode array was the limiting noise. In this circumstance a better signal-to-noise ratio should be obtained with a cooled CCD camera (see below). For neurons on the surface of the slice, where light scattering is less of a factor, the additional spatial resolution of the CCD camera might also be useful.

2. Action potentials from individual neurons
(Fig. 1, middle panel)

Aplysia *abdominal ganglion.* Nervous systems are made up of large numbers of neurons, and many of these are active during the generation of behaviors. The original motivation for developing optical methods was the hope that they could be used to record all of the action-potential activity of all the neurons in simpler invertebrate ganglia during behaviors (Davila *et al.,* 1973). Techniques that use
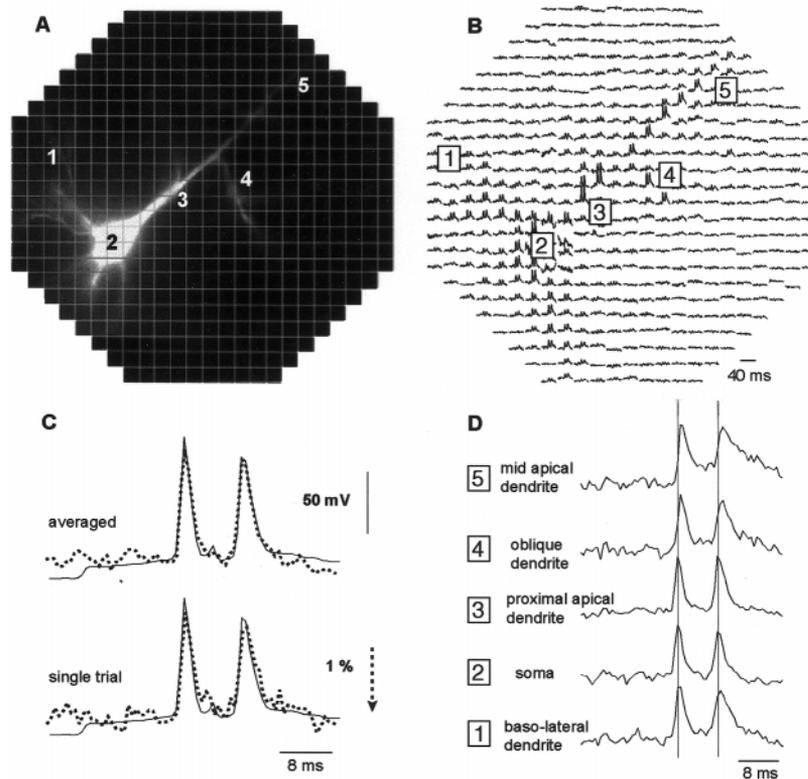
Figure 3. (A) Outline of the 464-element photodiode array superimposed over the fluorescent image of a pyramidal neuron. (B) Single-trial recording of action-potential-related optical signals. Each trace represents the output of one diode. Traces are arranged according to the disposition of the detectors in the array. Each trace represents 44 ms of recording. Each diode received light from a $14 \times 14\ \mu$m area in the object plane. Spikes were evoked by a somatic current pulse. (C) Comparison of electrical and optical recordings. Upper panel: spatial average of optical signals from eight individual diodes from the somatic region (dotted line) are superimposed on the electrical recording from the soma (solid line). Lower panel: same electrical signal compared with a single-trial optical recording. (D) Action potentials from individual detectors at different locations along the basal, oblique, and apical dendrites. Traces from different locations are scaled to the same height. The increasing delay between the signal from the somatic region and most proximal dendritic segments reflects the propagation velocity (0.22 m/s). At a distance of 230 μm from the soma, the half-width increased from 1.7 to 2.3 ms for the first spike and from 2.2 to 4.6 ms for the second spike in the burst. (Modified from Antic, Major, and Zecevic, 1999.)

microelectrodes are limited in that they can observe single-cell activity in only as many cells as one can simultaneously place electrodes (typically four or fewer neurons). Information about the activity of many cells is essential for understanding the roles of the individual neurons in generating behavior and for understanding how nervous systems are organized.

In the first attempt to use voltage-sensitive dyes in ganglia (Salzberg *et al.,* 1973), we were fortunate to be able to monitor activity in a *single* neuron because the photodynamic damage was severe and the signal-to-noise ratio small. Now, however, with better dyes and methods, the spike activity of hundreds of individual neurons can be recorded simultaneously (Zecevic *et al.,* 1989; Nakashima *et al.,* 1992). In the experiments described below, we measured the spike activity of up to 50% of the approximately

1000 cells in the *Aplysia* abdominal ganglion. Opisthobranch molluscs are favored for this kind of measurement because their central nervous systems have relatively few, relatively large neurons, and almost all of the cell bodies are fully invaded by the action potential. In addition, opisthobranch ganglia are organized with cell bodies on the outside and neuropil in the center. These characteristics are important because the dyes we used stained only the outer, cell body, layer, and the signal-to-noise ratio for action-potential recording would be reduced if the cell bodies did not have a full-sized action potential.

The 464-element silicon photodiode array was placed in the image plane formed by a microscope objective of $25 \times$ 0.4 NA. A single-pole high-pass and a four-pole low-pass Bessel filter in the amplifiers limited the frequency response to 1.5–200 Hz. We used the isolated siphon preparation

developed by Kupfermann *et al.* (1971). Considerable effort was made to find conditions that maximized the dye staining while causing minimal pharmacologic effects on the gill-withdrawal behavior. Intact ganglia were incubated in a 0.15 mg/ml solution of the oxonol dye RH155 (Fig. 9), or its diethyl analog, using a protocol developed by Nakashima *et al.* (1992). A light mechanical stimulation (1–2 g) was delivered to the siphon.

The signal-to-noise ratio in the measurements from individual cell bodies is optimal when the light from one cell body falls on one photodetector. With more photodetectors, the light from an individual cell is divided onto more than one detector (with a concomitant reduction in signal-to-noise ratio); with fewer photodetectors than cells, the light from more than one neuron falls on one detector, with a reduction in signal-to-noise ratio for the individual neurons. Thus an array of only 464 detectors is approximately optimal for a ganglion of 1000 neurons.

Because the image of a ganglion is formed on a rectilinear diode array, there is no simple correspondence between images of cells and photodetectors. The light from larger cell bodies falls on several detectors, and its activity is recorded as simultaneous events on neighboring detectors. In addition, because these preparations are multilayered, most detectors receive light from several cells. Thus, a sorting step is required to determine the activity in neurons from the spike signals on individual photodiodes. In the top right of Figure 4, the raw data from seven photodiodes from an array are shown. The activity of four neurons (shown in the raster diagram at the bottom) can account for the spike signals in the top section. Two problems are illustrated in this figure. Both arise from the signal-to-noise ratio. First, there may be an additional spike on detector 116 just before the stimulus (at the arrow), but the signal-to-noise ratio is not large enough to be certain. Second, following the stimulus, there is a great deal of activity, which will obscure small signals. Both problems suggest that the optical recordings are not complete; attempts to determine the completeness suggested that we were detecting the activity of about 50% of the neurons in the *Aplysia* abdominal ganglion (Wu *et al.,* 1994b). The fractional change in transmitted light ($\Delta I/I$) in these signals ranges from about 10^{-4} to 1.5×10^{-3}; the noise is substantially smaller.

The result of a complete analysis is shown in the raster diagram of Figure 5. The 0.5-s mechanical stimulus started at the time indicated by the line labeled "stim." The activity of 135 neurons was detected optically. Similar results have been obtained by Nakashima *et al.* (1992). Because this recording is only 50% complete, the actual number of activated neurons during the gill-withdrawal reflex was estimated to be about 300.

We were surprised at the large number of neurons that were activated by the light touch. Furthermore, a substantial number of the remaining neurons were likely to either be inhibited by the stimulus or receive a large subthreshold excitatory input. It is almost as if the *Aplysia* nervous system is designed so that every cell in the abdominal ganglion cares about this (and perhaps every) sensory stimulus. In addition, more than 1000 neurons in other ganglia are activated by this touch (Tsau *et al.,* 1994). Clearly, information about this very mild and localized stimulus is propagated widely in the *Aplysia* nervous system. These results impose a more pessimistic view of the present understanding of the neuronal basis of apparently simple behaviors in relatively simple nervous systems. Elsewhere we present arguments suggesting that the abdominal ganglion may function as a distributed system (Wu *et al.,* 1994a, b; Tsau *et al.,* 1994).

Guinea pig ganglion. Recently, similar measurements have been made from a vertebrate system, the ganglia of the submucous plexus of the guinea pig small intestine (Obaid *et al.,* 1999). It will be interesting to see if this vertebrate preparation also functions in a distributed manner.

3. Population signals (Fig. 1, right panel)

Turtle olfactory bulb. In the above experiments on *Aplysia* ganglia, each photodetector received light from one or a small number of neurons. In contrast, in measurements from a vertebrate brain (Fig. 1, right panel), each detector received light from a volume of the brain that includes thousands of neurons and processes. The resulting signal is a population average of the change in membrane potential of all of these cells. Populations signals have been recorded from many preparations (*e.g.,* Grinvald *et al.,* 1982a; Orbach and Cohen, 1983; Sakai *et al.,* 1985; Kauer, 1988; Cinelli and Salzberg, 1992; Albowitz and Kuhnt, 1993); the results from turtle are described because of our familiarity with them.

Odor stimuli induce stereotyped local field-potential responses consisting of sinusoidal oscillations of 10 to 80 Hz riding on top of a slow "DC" signal. Since their first discovery in the hedgehog (Adrian, 1942), odor-induced oscillations have been seen in phylogenetically distant species including locust (Laurent and Naraghi, 1994), turtle (Beuerman, 1975), and monkey (Hughes and Mazurowski, 1962). We measured the voltage-sensitive dye signal that accompanies these oscillations in the box turtle; our measurements allowed a more detailed visualization of the spatiotemporal characteristics of the oscillations.

The turtles were anesthetized by placing them in ice for 2 h, then a craniotomy was performed over the olfactory bulb. The dura and arachnoid mater were carefully removed to facilitate staining. The exposed olfactory bulb was stained by covering it with dye solution (RH414, 0.02–0.2 mg/ml) for 60 min; excess dye was washed away with turtle saline. The odor output from the olfactometer was more-or-less square and had a latency of about 100 ms from the onset
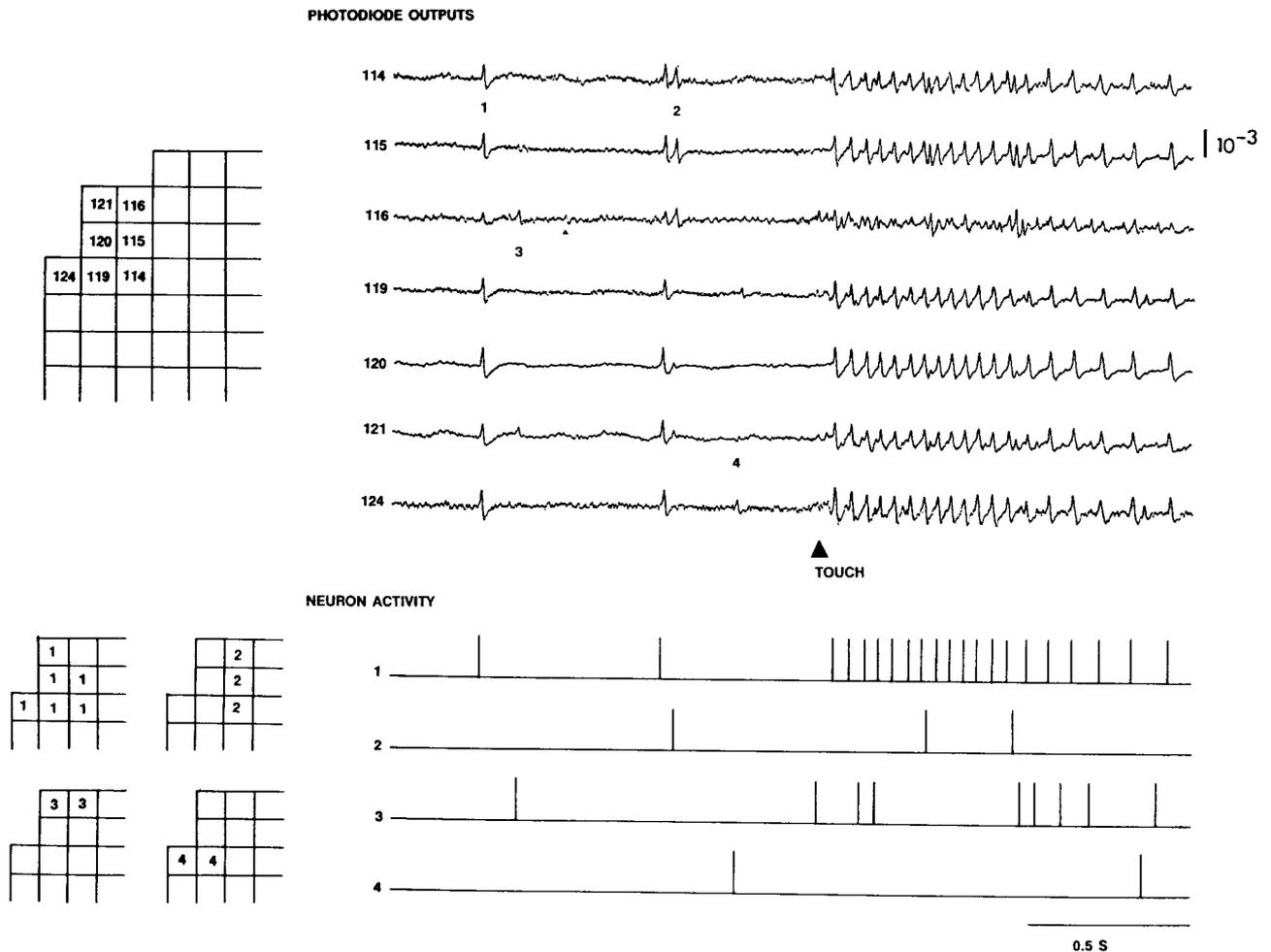
Figure 4. Optical recordings from a portion of a photodiode array from an *Aplysia* abdominal ganglion. The drawing to the left represents the relative position of the detectors whose activity is displayed. In the top right, the original data from seven detectors are illustrated. The numbers to the right of each trace identify the detector from which the trace was taken. The bottom section shows the raster diagram illustrating the results of our sorting of these data into the spike activity of four neurons. At the number 1 in the top section there are synchronously occurring spike signals on all seven detectors. A synchronous event of this kind occurs more than 20 times; we presume that each event represents an action potential in one relatively large neuron. The activity of this cell is represented by the vertical lines on trace 1 of the bottom section. The activity of a second cell is indicated by small signals at the number 4 on 119 and its neighbor, 124. The activity of this cell is represented by the vertical lines on trace 4 of the bottom section. The activity of neurons 2 and 3 was similarly identified. (Modified from Zecevic *et al.,* 1989.)

of the command pulse to the solenoid controlling odor delivery.

We optimized the optics for measurements of epifluorescence at low magnification. In this circumstance the intensity reaching the objective image plane is proportional to the fourth power of the numerical aperture (NA) of the objective (Inoué, 1986). Because conventional microscope optics have small numerical apertures at low magnifications, we assembled a microscope (macroscope) based on a 25-mm focal length, 0.95 f, C-mount, camera lens (used with the C-mount end facing the preparation) (Salama, 1988; Ratzlaff and Grinvald, 1991; Kleinfeld and Delaney, 1996).

With a magnification of 4×, the intensity reaching the photodetector was 100 times larger with this lens than with a conventional 4×, 0.16 NA microscope lens. Additional details of the apparatus are given in Wu and Cohen (1993), Wu *et al.* (1998), and Lam *et al.* (2000).

With this 4× magnification each detector will receive light from an area of the object plane that is $170 \times 170 \ \mu m^2$. Because of light scattering by the preparation (see Fig. 12), it would not be possible to achieve better spatial resolution even if the camera had more pixels.

In Figure 6, the recordings from seven selected diodes in a single trial are shown. The location of these diodes is

B. RESPONSE TO SIPHON TOUCH IN APLYSIA
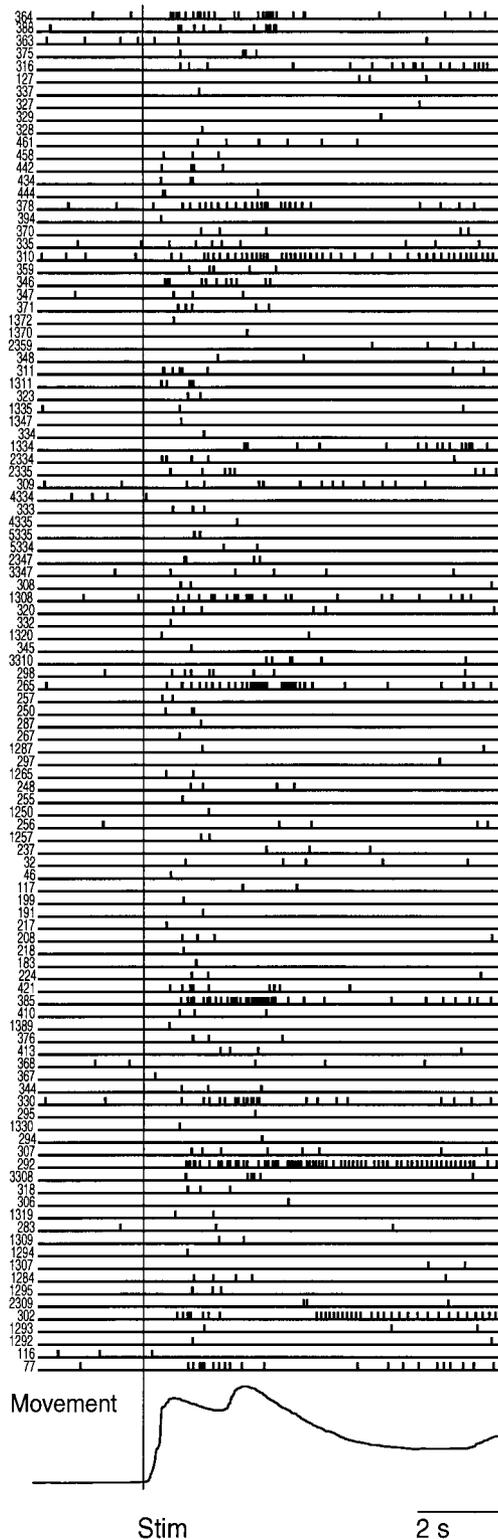
Figure 5. Raster diagram of the action-potential activity recorded optically from an *Aplysia* abdominal ganglion during a gill-withdrawal reflex. The 0.5-s touch to the siphon began at the time of the line labeled STIM. In this recording, activity in 135 neurons was measured. We think this recording is incomplete and that the actual number of active neurons was between 250 and 300. Most neurons are activated by the touch, but one, #4334 (about 1/3 down from the top), was inhibited. This inhibition was seen in repeated trials in this preparation. (Modified from Wu *et al.*, 1994b.)

indicated on the image by the numbered squares on the left. In rostral locations (detectors 1 and 2), we found a single oscillation with a relatively high frequency. On a diode from a middle location (detector 4) there was a relatively brief, short-latency oscillation, and on a diode from the caudal bulb (detector 7), the oscillation was of a lower frequency and a long latency. In areas between two regions, the recorded oscillations were combinations of two signals: rostral/middle in detector 3 and middle/caudal in detectors 5 and 6. We named the three oscillations *rostral, middle,* and *caudal.* The fractional change in fluorescence ($\Delta F/F$) in these three signals ranged from about 2×10^{-4} to 10^{-3}; the noise was substantially smaller. In addition, a DC signal, which appears as a single peak after high-pass filtering in Figure 6, was observed over most of the ipsilateral olfactory bulb. Figure 7A shows the time course of an unfiltered recording. Following the start of the odor command pulse, the optical signal rose to a plateau and then continued for several seconds. After a short delay, the rostral oscillations appeared on the DC response. The rostral oscillation had a long latency and a high frequency. The middle oscillation had a short latency and a frequency that was similar to the rostral oscillation. The caudal oscillation had a lower frequency and the longest latency. In addition to differences in frequency and latency, the three oscillations also had different shapes—the rostral and caudal oscillations had relatively sharp peaks, whereas the middle oscillation was more sinusoidal.

Figure 7 shows the time courses of the signals from four detectors from this trial together with multiple-frame images indicating the position and propagation during one cycle of each oscillation. The rostral, middle, and caudal oscillations are clearer after the DC signal was reduced with a high-pass filter (Fig. 7B, C, D). In these multi-frame images, the red color and the area enclosed by the black line indicate the areas in which the signals are larger than 80% and 20% of the maximum signal respectively. The DC signal covered most of the olfactory bulb. The rostral signal (D) propagated in the caudal direction, the middle signal (B) did not appear to propagate, and the caudal signal (C) propagated in a lateral-caudal direction. Prechtl *et al.* (1997) also found that propagation was a characteristic of many oscillations in the turtle visual cortex.

Oscillations are not restricted to the olfactory system. Despite their ubiquity, the roles and functions of oscillation are not well understood. Nevertheless, their ubiquity and the large number of neurons that they involve make it reason-
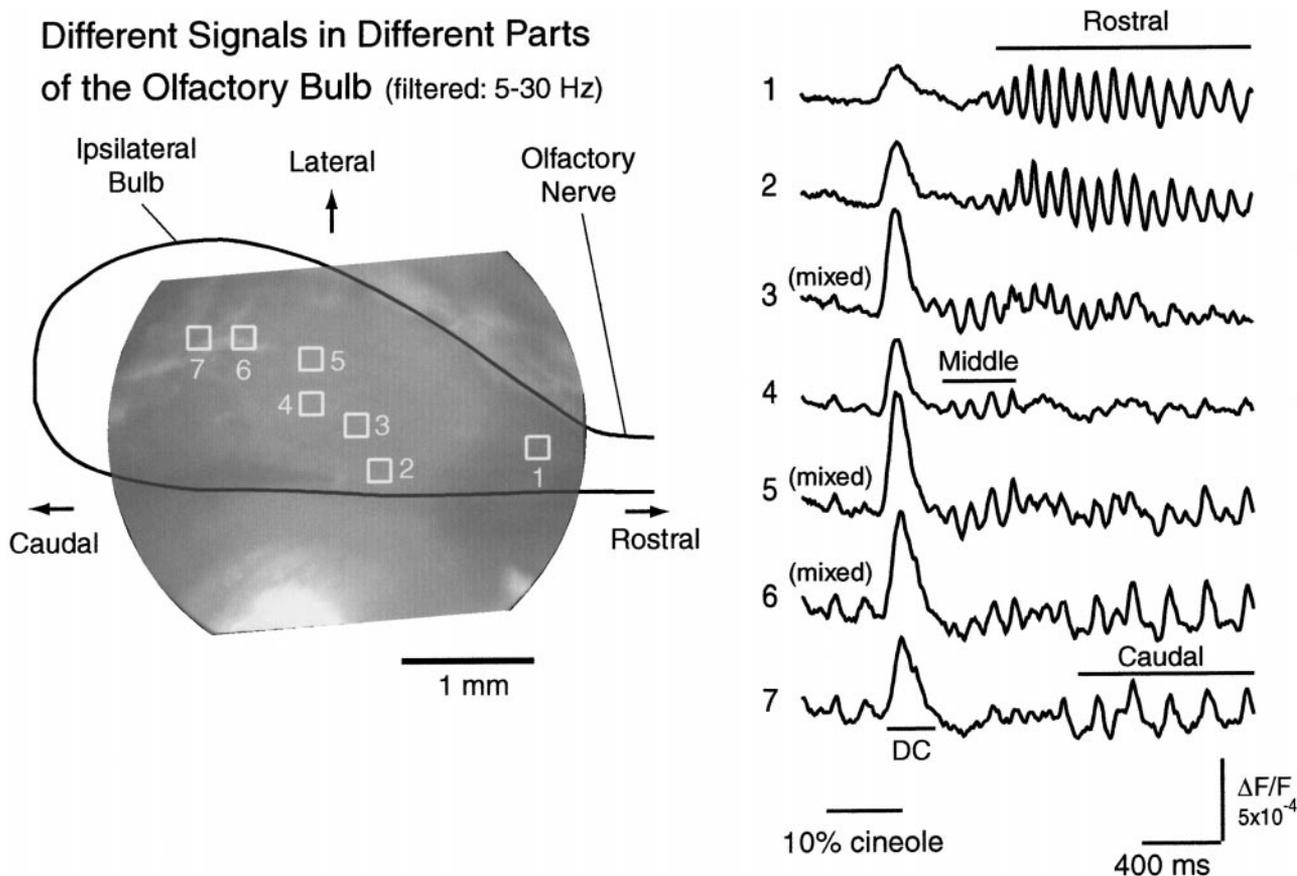
Figure 6. Simultaneous optical recordings from seven areas of an olfactory bulb. An image of the olfactory bulb is shown on the left. Signals from seven selected pixels are shown on the right. The positions of these pixels are labeled with squares and numbers on the image of the bulb. All seven signals have a filtered version of the DC signal at the time indicated by the bar labeled DC. The oscillation in the rostral region has a high frequency and relatively long latency and duration (detectors 1 and 2). The oscillation from the middle region has a high frequency and short latency and duration (detector 4). The oscillation from the caudal region has a lower frequency and the longest latency (detector 7). The signal from detectors between these regions (3, 5, and 6) appears to contain a mixture of two components. The horizontal line labeled "10% cineole" indicates the time of the command pulse to the odor solenoid. The data are filtered by a high-pass digital RC (5 Hz) and low-pass Gaussian (30 Hz) filters. (Modified from Lam *et al.,* 2000.)

able to speculate that oscillations may be important in perception. Our data show that the odor-induced oscillations in the olfactory bulb are substantially more complicated than had been anticipated and that multiple functional population domains are processing olfactory input in parallel.

In vivo *mammalian brain.* Population signals are more difficult to measure from *in vivo* mammalian preparations than from the turtle because the noise from the heartbeat and respiration is greater and because staining is more difficult. Two methods for reducing the movement artifacts from the heartbeat are, together, quite effective. First, a subtraction procedure is used in which two recordings are made but only one of the trials has a stimulus (Orbach *et al.,* 1985). Both recordings are triggered from the upstroke of the electrocardiogram, so they should have similar heartbeat noise. When the trial with-

out the stimulus is subtracted from the trial with the stimulus, the heartbeat artifact is reduced. Second, an airtight chamber is fixed onto the skull surrounding the craniotomy (Blasdel and Salama, 1986). When this chamber is filled with silicon oil and closed, the movements due to heartbeat and respiration are substantially reduced. In combination, these methods reduce the noise from movement artifacts enough that it is no longer the main source of noise in the measurements.

Methods

The three examples given above involve fractional intensity changes that ranged from 10^{-4} to 3×10^{-2}. To measure these signals, the noise in the measurements had to be an even smaller fraction of the resting intensity. In the sections that

Locations and propagation (filtered: DC:0.1-30Hz ; Osc: 5Hz-30Hz)

A. DC

65% 80%

1 mm

B. Middle

frame / 8 ms

1 mm

C. Caudal

10 %
cineole

D. Rostral

frame / 8ms
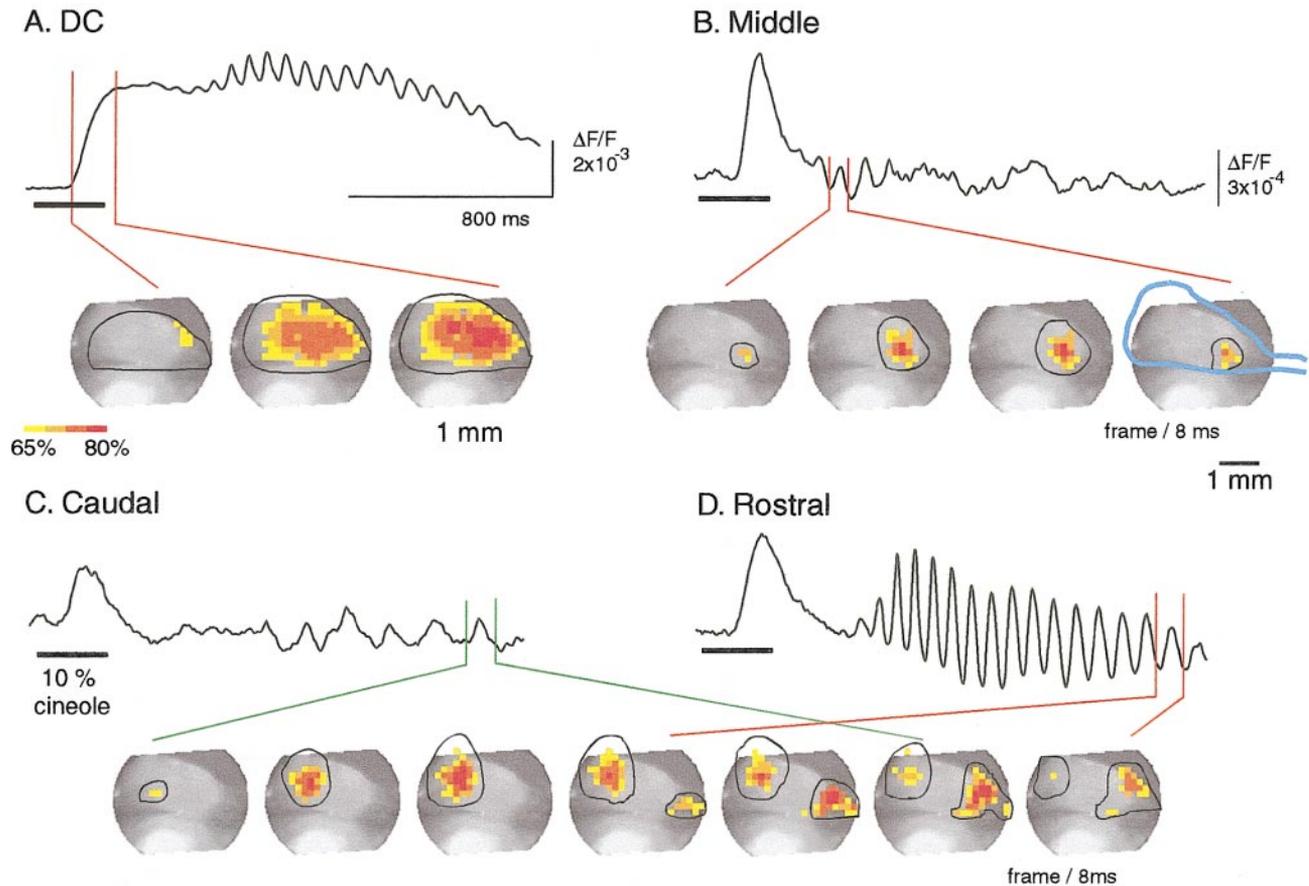
Figure 7. The locations and propagation of the four components from the trial shown in Figure 6. Multiframe pseudo-color displays of the signals are overlaid on the image of the olfactory bulb. The red color and the black contour lines label the areas where the signals are larger than 80% and 20% of the peak. The DC component in this animal covers almost the entire bulb. The other three panels show the position and propagation of one cycle (indicated by the red and green lines) of the three different oscillations. The black horizontal bars indicate the time of the odor command-pulse. The data are filtered by a high-pass digital RC (5 Hz) and low-pass Gaussian (30 Hz) filters. (Modified from Lam *et al.,* 2000.)

follow, some of the considerations necessary to achieve such a low noise are outlined. Two topics that were discussed in earlier reviews will not be covered here: first, evidence showing that these optical signals are fast and potential-dependent; second, evidence that pharmacological effects and photodynamic damage resulting from the voltage-sensitive dyes are manageable (see, *e.g.,* Cohen and Salzberg, 1978; Waggoner, 1979; Salzberg, 1983; Sakai *et al.,* 1985; Cohen and Lesher, 1986; Grinvald *et al.,* 1988; Momose-Sato *et al.,* 1995).

Signal Type

Sometimes it is possible to decide in advance which kind of optical signal will give the best signal-to-noise ratio, but in other situations an experimental comparison is necessary. The choice of signal type often depends on the optical characteris-

tics of the preparation. Birefringence signals are relatively large in preparations that, like axons, are cylindrical and have a radial optic axis. However, in preparations with spherical symmetry (*e.g.,* cell soma), the birefringence signals in adjacent quadrants cancel (Boyle and Cohen, 1980).

Thick preparations (*e.g.,* mammalian cortex) also dictate the choice of signal. In this circumstance transmitted light measurements are not easy (a subcortical implantation of a light guide would be necessary), and the small size of the absorption signals that are detected in reflected light (Ross *et al.,* 1977; Orbach and Cohen, 1983) means that fluorescence is optimal (Orbach *et al.,* 1985).

Another factor that affects the choice of absorption or fluorescence is that the signal-to-noise ratio in fluorescence is more strongly degraded by dye bound to extraneous
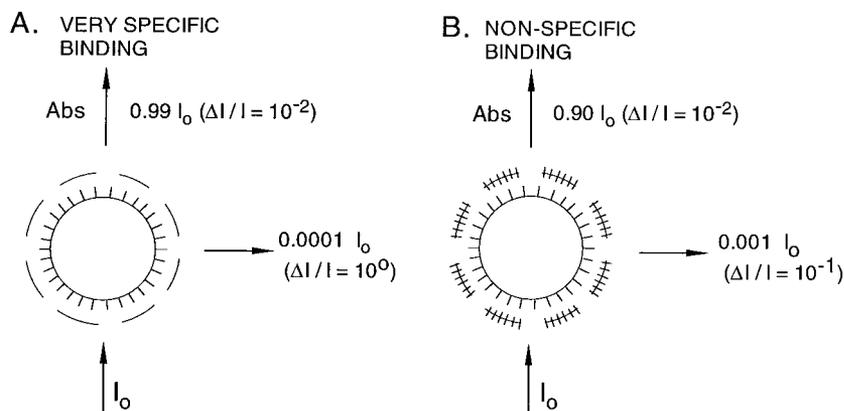
Figure 8. (A) The light transmission and fluorescence intensity when only a neuron binds dye and (B) when both the neuron and extraneous material binds dye. In (A), assuming that one dye molecule is bound for every 2.5 phospholipid molecules, 0.99 of the incident light is transmitted. If a change in membrane potential causes the dye to disappear, the fractional change in transmission is 1%, but in fluorescence it is 100%. In (B), nine times as much dye is bound to extraneous material. Now the transmitted intensity is reduced to 0.9, but the fractional change is still 1%. The fluorescence intensity is increased 10-fold, and therefore the fractional change is reduced by the same factor. Thus, extraneously bound dye degrades fluorescence fractional changes and signal-to-noise ratios more rapidly. (Redrawn from Cohen and Lesher, 1986.)

material. Figure 8 illustrates a spherical cell surrounded by extraneous material. In Figure 8A, dye is bound only to the cell; in 8B, there is 10 times as much dye bound to extraneous material. To calculate the transmitted intensity in Figures 8A and B, we assume that there is one dye molecule for every 2.5 phospholipid molecules and a large extinction coefficient (10^5). The amount of light absorbed by the cell is still only 0.01 of the incident light I_o and thus the transmitted light is 0.99 I_o. Thus, even if this dye completely disappeared due to a change in potential, the fractional change in transmission, $\Delta I/I_o$, would be only 1% (10^{-2}). The amount of light reaching the photodetector in fluorescence is much lower, say 0.0001 I_o, but even so, disappearance of dye would result in a 100% decrease in fluorescence, a fractional change of 10^0. Thus, in situations in which dye is bound only to the cell membrane and only one cell is in the light path, the fractional change in fluorescence is much larger than the fractional change in transmission.

However, the relative advantage of fluorescence is reduced if dye binds to extraneous material. When 10 times as much dye is bound to the extraneous material as was bound to the cell membrane (Fig. 8B), the transmitted intensity is reduced to about 0.9 I_o, but the fractional change in transmission is nearly unaffected. In contrast, the resting fluorescence is now higher by a factor of 10, and the fractional fluorescence change is reduced by the same factor. It does not matter whether the extraneous material is connective tissue, glial membrane, or neighboring neuronal membranes.

In Figure 8B, the fractional change in fluorescence was still larger than in transmission. However, in fluorescence, the light intensity was about 10^3 smaller, which reduces the signal-to-noise ratio. Partly because of the signal degradation due to extraneous dye, fluorescence signals have most often been used in monitoring activity from tissue-cultured neurons. Both fluorescence and absorption signals have been used in measurements from ganglia and brain slices. Fluorescence has always been used in measurements from intact brains.

Dyes

Several voltage-sensitive dyes have been used to monitor changes in membrane potential in a variety of preparations. Figure 9 illustrates four different chromophores: for each, about 100 analogs were synthesized in an attempt to optimize the signal-to-noise ratio that can be obtained in a variety of preparations. This screening was made possible by the efforts of three laboratories: Jeff Wang, Ravender Gupta, and Alan Waggoner, then at Amherst College; Rina Hildesheim and Amiram Grinvald at the Weizmann Institute; and Joe Wuskell and Leslie Loew at the University of Connecticut Health Center.

For each of the four chromophores, 10 or 20 dyes gave roughly the same signal size on squid axons (Gupta *et al.,* 1981). Unfortunately, they often gave very different responses on other preparations, so that several dyes had to be tested. Often, dyes that worked well in squid did poorly in other preparations because they failed to penetrate through connective tissue or along intercellular spaces to the membrane of interest. Others dyes appeared to have a relatively low affinity for neuronal *versus* non-neuronal tissue. Finally, in some cases, the dye penetrated well and the stain-
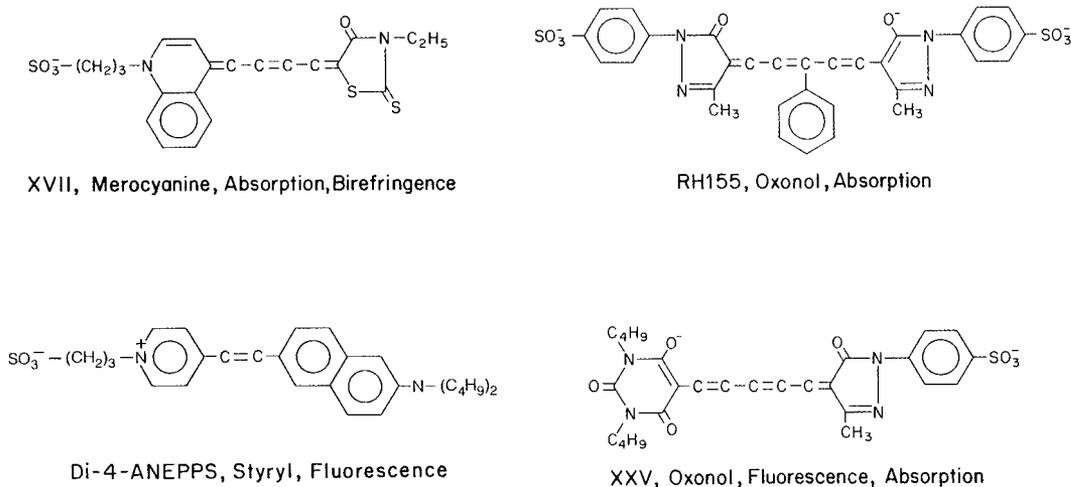
Figure 9.   Examples of four different chromophores that have been used to monitor membrane potential. The merocyanine dye, XVII (WW375), and the oxonol dye, RH155, are commercially available as NK2495 and NK3041 from Nippon Kankoh-Shikiso Kenkyusho Co. Ltd., Okayama, Japan. The oxonol, XXV (WW781) and styryl, di-4-ANEPPS, are available commercially as dye R-1114 and D-1199 from Molecular Probes, Junction City, Oregon.

ing appeared to be specific, but nonetheless the signals were small.

The voltage-sensitive dye signals discussed in this article are presented as the fractional intensity change ($\Delta I/I$). These signals give information about the time course of the potential change but no direct information about its magnitude. In some instances, indirect information about the magnitude of the voltage change can be obtained (*e.g.,* Orbach *et al.,* 1985; Delaney *et al.,* 1994; Antic and Zecevic, 1995). Another approach is the use of ratiometric measurements at two independent wavelengths (Gross *et al.,* 1994). However, to determine the amplitude of the voltage change from a ratio measurement, one must know the fraction of the fluorescence that results from dye not bound to active membrane, a requirement that is only approximately met in special circumstances (*e.g.,* tissue culture).

Measuring Technology

Noise.

1. Shot noise. The accuracy with which light can be measured is limited by the shot noise arising from the statistical nature of photon emission and detection. The number of photons emitted per unit time fluctuates, and if an ideal light source (tungsten filament at 3300°F) emits an average of 10^{16} photons/ms, the root-mean-square (RMS) deviation in the number emitted is the square root of this number, or 10^8 photons/ms. The signal-to-noise ratio is directly proportional to the square root of the number of measured photons and inversely proportional to the

square root of the bandwidth of the photodetection system (Braddick, 1960; Malmstadt *et al.,* 1974). The basis for the square-root dependence on intensity is illustrated in Figure 10: in 10A, the result of using a random number table to distribute 20 photons into 20 time windows is shown; in 10B, the same procedure was used to distribute 200 photons into the same 20 bins. Relative to the average light level, there is more noise in the top trace (20 photons) than in the bottom trace (200 photons). The measured signal-to-noise ratios are listed on the right side of Figure 10, and we show that the improvement from A to B is similar to that expected from the square-root relationship. This square-root relationship is indicated by the dotted line in Figure 11, which plots the light intensity divided by the noise in the measurement *versus* the light intensity. In a shot-noise–limited measurement, the signal-to-noise ratio can only be improved by (a) increasing the illumination intensity, (b) increasing the light-gathering efficiency of the measuring system, or (c) reducing the bandwidth.

Because only a small fraction of the 10^{16} photons/ms emitted by a tungsten filament is measured, a signal-to-noise ratio of 10^8 (see above) cannot be achieved. A partial listing of the light losses follows. A 0.9-NA lamp collector lens would collect 0.1 of the light emitted by the source. Only 0.2 of that light is in the visible wavelength; the remainder is infrared (heat). Limiting the incident wavelengths to those that have the signal means that only 0.1 of the visible light is used. Thus, the light reaching the preparation might typically be reduced to 10^{13} photons/ms. If the
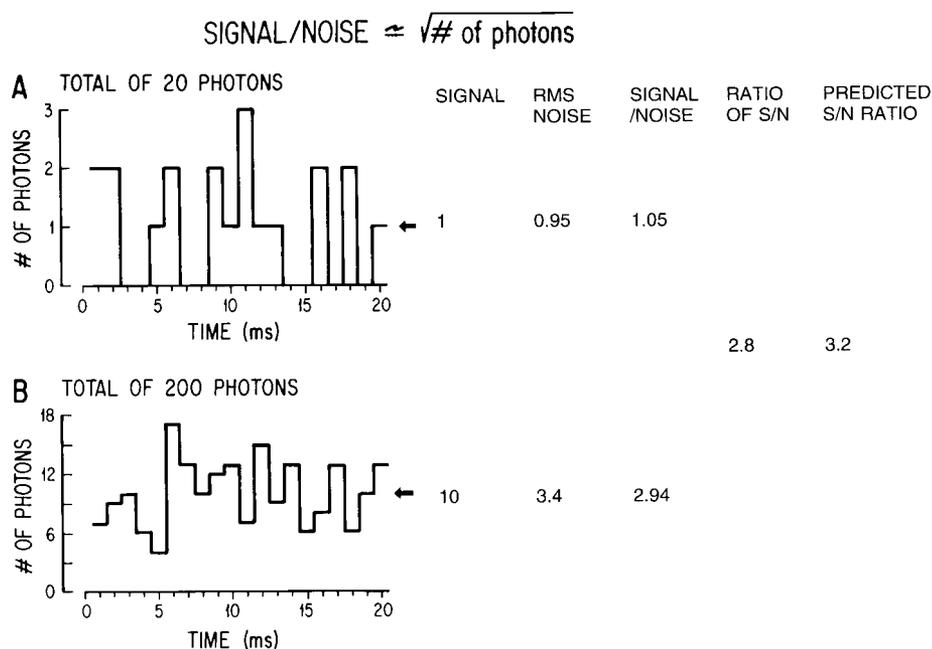
Figure 10. Plots of the results of using a table of random numbers to distribute 20 photons (top, A) or 200 photons (bottom, B) into 20 time bins. The result illustrates that when more photons are measured, the signal-to-noise ratio is improved. On the right, the signal-to-noise ratio is measured for the two results. The ratio of the two signal-to-noise ratios was 0.43, which is close to the value predicted by the relationship that the signal-to-noise ratio is proportional to the square root of the measured intensity. (Redrawn from Wu and Cohen, 1993.)

light-collecting system that forms the image is efficient (*e.g.,* in an absorption measurement), about 10^{13} photons/ms reach the image plane. (In a fluorescence measurement much less light is measured because (a) only a fraction of the incident photons are absorbed by the fluorophores, (b) only a fraction of the absorbed photons appear as emitted photons, and (c) only a fraction of the emitted photons are collected by the objective.) If the camera has a quantum efficiency of 1.0, then, in absorption, a total of 10^{13} photoelectrons/ms are measured. With a camera of 1000 pixels, there are 10^{10} photoelectrons/ms/pixel. The shot noise is 10^5 photoelectrons/ms/pixel; thus the best that can be expected is a relative noise 10^{-5} of the resting light (a signal-to-noise ratio of 100 db). The extra light losses in a fluorescence measurement further reduce the maximum obtainable signal-to-noise ratio.

One way to compare the performance of camera systems and to understand their deviations from optimal (shot-noise–limited) is to determine the light intensity divided by the noise in the measurement and plot that value against the number of photons reaching the photodetector. The dotted line in Figure 11 is such a plot for the ideal case. At high light intensities this ratio is large, and thus small changes

in intensity can be detected. For example, at 10^{10} photons/ms, a fractional intensity change of 0.1% can be measured with a signal-to-noise ratio of 100. On the other hand, at low intensities, the ratio of intensity divided by noise is small, and only large signals can be detected. For example, at 10^4 photons/ms, the same fractional change of 0.1% can be measured with a signal-to-noise ratio of 1 only after averaging 100 trials.

In addition, Figure 11 compares the performance of two camera systems, a photodiode array (solid lines) and a cooled CCD camera (dashed lines), with the shot-noise ideal. The photodiode array approaches the shot-noise limitation over the range of intensities from 3×10^6 to 10^{10} photons/ms. This is the range of intensities obtained in absorption measurements and fluorescence measurements on *in vitro* slices and intact brains. On the other hand, the cooled CCD camera approaches the shot-noise limit over the range of intensities from 5×10^3 to 5×10^6 photons/ ms. This is the range of intensities obtained from fluorescence experiments on individual cells and neurons. In the discussion that follows we indicate the aspects of the measurements and the characteristics of the two camera systems that cause them to deviate from the shot-noise ideal. The camera sys-
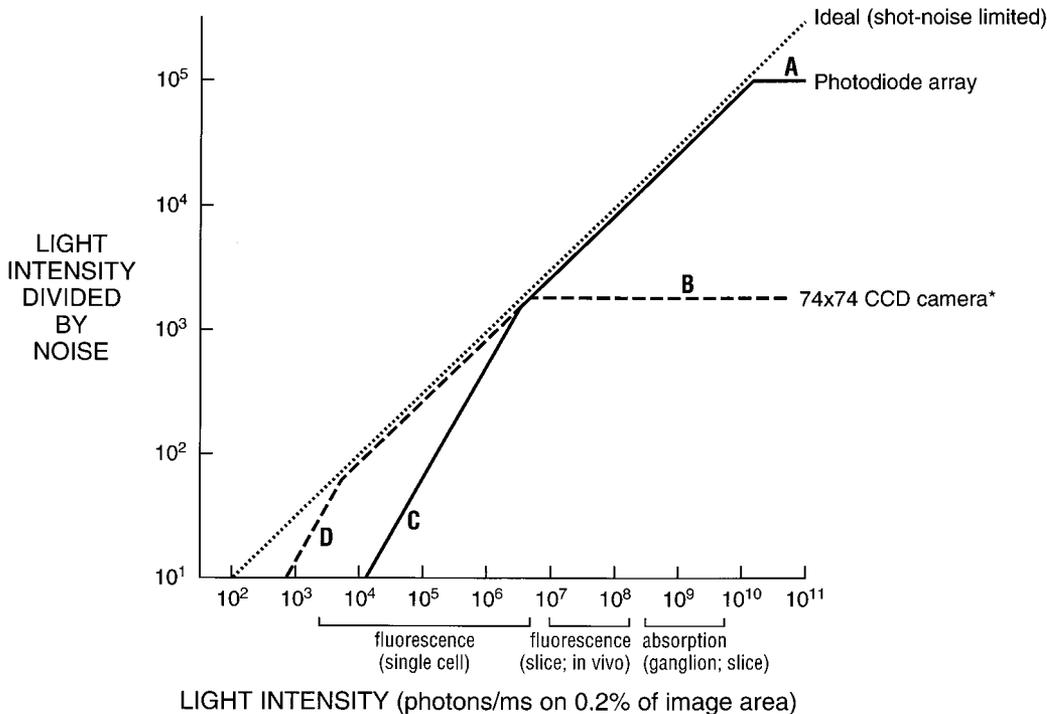
Figure 11. The ratio of light intensity divided by the noise in the measurement as a function of light intensity in photons per millisecond for each 0.2% of the object plane. The theoretical optimum signal-to-noise ratio (dotted line) is the shot-noise limit. Two camera systems are shown, a photodiode array with 464 pixels (solid lines) and a cooled, back-illuminated CCD camera with a 2-kHz frame rate and a 74×74 pixel resolution (dashed lines). The photodiode array provides an optimal signal-to-noise ratio at higher intensities, whereas the CCD camera is better at lower intensities. The approximate light intensity per detector in fluorescence measurements from a single neuron, fluorescence measurements from a slice or *in vivo* preparation, and in absorption measurements from a ganglion or a slice is indicated along the *x* axis. The signal-to-noise ratio for the photodiode array falls away from the ideal at high intensities (A) because of extraneous noise and at low intensities (C) because of dark noise. The lower dark noise of the cooled CCD allows it to function at the shot-noise limit at lower intensities until read noise dominates (D). The CCD camera saturates at intensities above 5×10^6 photons/ms/0.2% of the object plane.

tems illustrated in Figure 11 have relatively good dark noise and saturation characteristics; other cameras would be dark-noise–limited at higher light intensities and would saturate at lower intensities.

2. Extraneous noise. A second type of noise, termed extraneous, or technical, noise, is more apparent at high light intensities at which the sensitivity of the measurement is high because the fractional shot noise and dark noise are low. One source of extraneous noise is fluctuations in the output of the light source (see below). Two other sources are vibrations and movement of the preparation. A number of precautions for reducing vibrational noise have been described (Salzberg *et al.,* 1977; London *et al.,* 1987). The pneumatic isolation mounts on many vibration isolation tables reduce vertical vibrations more efficiently than they reduce horizontal movements. We now use air-filled tubes made of soft

rubber (Newport Corp, Irvine, CA). Nevertheless it has been difficult to reduce vibrational noise to less than 10^{-5} of the total light. With this amount of vibrational noise, increases in measured intensity beyond 10^{10} photons/ms would not improve the signal-to-noise ratio. Because of vibrational noise, the performance of the photodiode array system is shown reaching a ceiling in Figure 11 (segment A, solid line).

3. Dark noise. Dark noise degrades the signal-to-noise ratio at low light levels. Because the CCD camera is cooled, its dark noise is substantially lower than that of the photodiode array system. The excess dark noise in photodiode array explains why segment C in Figure 11 is substantially to the right of segment D.

Light sources. Three kinds of sources have been used. Tungsten filament lamps are a stable source, but their intensity

is relatively low, particularly at wavelengths less than 450 nm. Arc lamps are somewhat less stable but can provide more intense illumination. Until recently, measurements made with laser illumination have been substantially noisier.

1. Tungsten filament lamps. It is not difficult to provide a power supply stable enough that the output of the bulb fluctuates by less than 1 part in 10^5. In absorption measurements, where the fractional changes in intensity are relatively small, only tungsten filament sources have been used. In contrast, fluorescence measurements often have larger fractional changes that will better tolerate light sources with systematic noise, and the measured intensities are lower, making improvements in signal-to-noise ratio from brighter sources attractive.

2. Arc lamps. Opti-Quip, Inc., provides 150-W and 250-W xenon power supplies, lamp housings, and arc lamps with noise in the range of 1 part in 10^4. At 520 ± 45 nm, the 150-W bulb yielded 2–3 times more light than a tungsten filament bulb, and the 250-W bulb was 2–3 times brighter than the 150-W bulb. The extra intensity is especially useful for fluorescence measurements from single neurons. If the dark noise is dominant, then the signal-to-noise ratio improves linearly with intensity; if the shot noise is dominant, the ratio improves as the square root of intensity (Fig. 11).

3. Lasers. It has been possible to take advantage of one characteristic of laser sources. In preparations with minimal light scattering, the laser output can be focused onto a small spot, allowing measurement of membrane potential from small processes in tissue-cultured neurons (Bullen *et al.,* 1997). However, there may be excess noise due to laser speckle (Dainty, 1984).

Optics.

1. Numerical aperture. The need to maximize the number of measured photons has also been a dominant factor in the choice of optical components. In epifluorescence, both the excitation light and the emitted light pass through the objective, and the intensity reaching the photodetector is proportional to the fourth power of the numerical aperture (Inoue, 1986).

2. Objective efficiency. Direct comparison of the intensity reaching the image plane has shown that the light-collecting efficiency of an objective is not completely determined by the stated magnification and NA. Lenses of the same specification can differ by a factor of 5. We presume that these differences depend on the number of lenses, the coatings, and absorbances of glasses and cements. We recommend empirical tests of several lenses for efficiency.
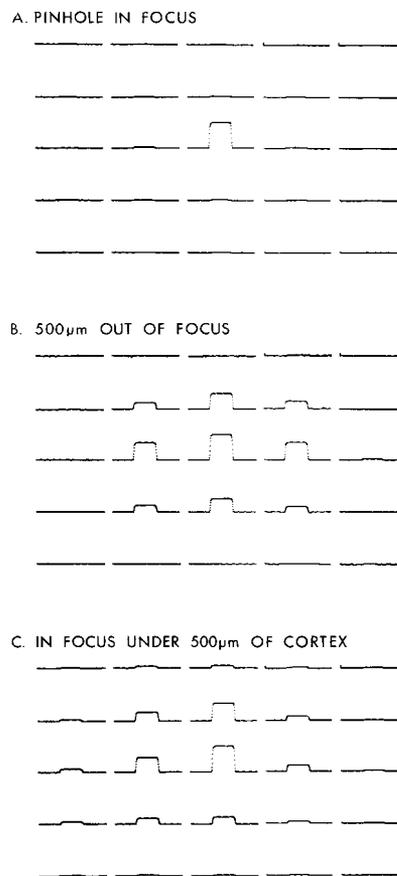
Figure 12. Effects of focus and scattering on the distribution of light from a point source onto the array. (A) A 40-μm pinhole in aluminum foil covered with saline was illuminated with light at 750 nm. The pinhole was in focus. More than 90% of the light fell on one detector. (B) The stage was moved downward by 500 μm. Light from the out-of-focus pinhole was now seen on several detectors. (C) The pinhole was in focus but covered by a 500-μm slice of salamander cortex. Again the light from the pinhole was spread over several detectors. A 10 $\times$ 0.4 NA objective was used. Kohler illumination was used before the pinhole was placed in the object plane. The recording gains were adjusted so that the largest signal in each of the three trials would be approximately the same size in the figure. (Redrawn from Orbach and Cohen, 1983.)

3. Depth of focus. Salzberg *et al.* (1977) determined the effective depth of focus for a 0.4-NA objective lens by recording an optical signal from a neuron when it was in focus and then moving the neuron out of focus by various distances. The neuron had to be moved 300 μm out of focus to reduce the size of the signal by 50%. (This result is obtained only when the diameter of the neuron image and the diameter of the detector are similar.) With 0.5-NA optics, a 50% reduction was obtained at 100 μm out of focus (Kleinfeld and Delaney, 1996).

4. Light scattering and out-of-focus light. Light scattering can limit the spatial resolution of an optical measurement. London *et al.* (1987) measured the
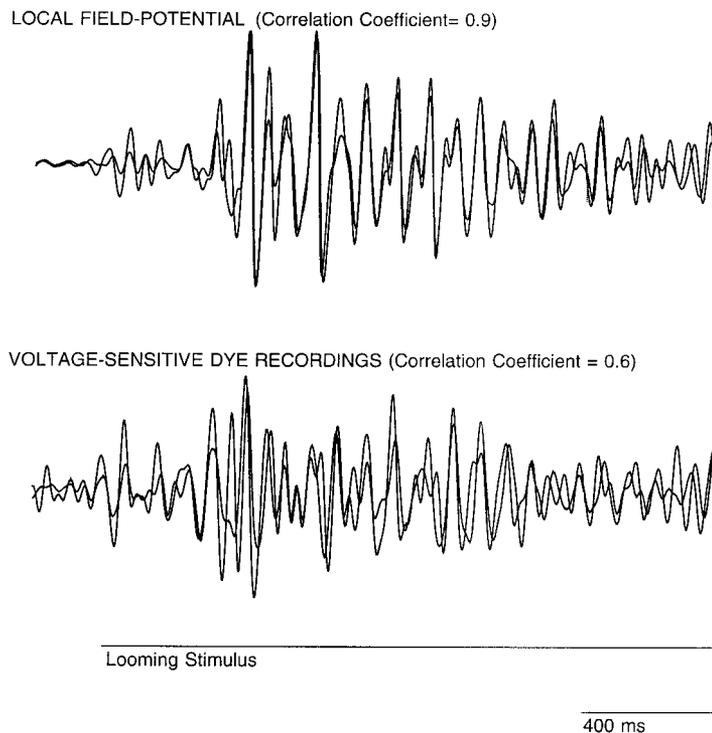
scattering of 705-nm light in *Navanax* buccal ganglia. Inserting a ganglion in the light path caused light from a 30-μm spot to spread so that the diameter of the circle of light that included intensities greater than 50% of the total was roughly 50 μm. The spread was greater, to about 100 μm, with light of 510 nm. Figure 12 illustrates the results of similar experiments on the olfactory bulb of the salamander. When no tissue is present, essentially all of the light (750 nm) from a small spot falls on one detector (top of figure); when a 500-μm-thick slice of olfactory bulb is present, the light from the small spot is spread to about 200 μm (bottom of figure). Scattering appears to be greater with mammalian cortex than with olfactory bulb. Thus, light scattering blurs signals in adult vertebrate preparations.

A second source of blurring is signal from regions that are out of focus. For example, if the active region is a cylinder (a column) perpendicular to the plane of focus, and the objective is focused at the middle of the cylinder, then the light from the in-focus plane has the correct diameter at the image plane. However, the light from the regions above and below is out of focus, and its diameter is too large. The middle section of Figure 12 illustrates the effect of moving the small spot of light 500 μm out of focus: the light is spread to about 200 μm. Thus, in preparations with considerable scattering or with out-of-focus signals, the spatial resolution may be limited by the preparation and not by the number of pixels in the imaging device.

Comparison of voltage-sensitive dye and local field potential measurements of population signals. The results in Figure 12 suggest that the spatial resolution of a population signal in a vertebrate brain is limited to about 200 μm by light scattering and out-of-focus signals. This spatial resolution is substantially better than that obtained by recording local field potentials from the surface of the brain. Because the current sources driving these potentials can be below the surface, the spatial patterns are smoothed by the volume-conductor properties of the cortical tissue. Freeman (1978)

SPATIAL RESOLUTION OF LFP AND OPTICAL RECORDINGS;
TWO LOCATIONS ON CORTEX SEPARATED BY 2.3 MM.

LOCAL FIELD-POTENTIAL (Correlation Coefficient= 0.9)

VOLTAGE-SENSITIVE DYE RECORDINGS (Correlation Coefficient = 0.6)

Looming Stimulus

400 ms

Figure 13. Comparison of simultaneous optical and local-field-potential recordings from two positions on turtle visual cortex that were separated by 2.3 mm. The top pair of superimposed traces are the local-field-potential recordings from the two sites. The bottom pair of traces are the voltage-sensitive-dye recordings from the two sites. There is much less overlap in the optical recordings. Thus, the voltage-sensitive dye recordings have better spatial resolution. Both sets of recordings were band-pass filtered (10–30 Hz). (J. Prechtl, L. B. Cohen, and D. Kleinfeld, unpubl. data.)

reported that spatial Fourier transforms from local field potential measurements had a sharp cutoff at about 1 cycle/mm, suggesting a resolution on the order of 1 mm. Similarly, in the frequency range below 30 Hz, Bullock and McClune (1989) reported a correlation of about 0.9 between two local field potential electrodes spaced 2–3 mm apart on the surface of the brain.

We compared the spatial resolution of the two kinds of measurements by examining simultaneous pairs of recordings from two positions on turtle visual cortex that were separated by 2.3 mm. The top pair of superimposed traces in Figure 13 are the local field potentials. The recordings from the two sites show considerable overlap: the correlation coefficient was 0.9. The bottom pair of traces are the voltage-sensitive dye recordings. These show less overlap—their correlation coefficient was 0.6. Thus, the spatial differences are less blurred with the optical recordings than with the electrode recordings.

We estimated the relative spatial resolution of the two methods by determining the distance on the cortex at which the correlation coefficients would be equal for a pair of voltage-sensitive dye recordings and a pair of local field potential recordings. In six trials from two preparations the correlation coefficients were equal when the two optical measurements were a distance apart that was 0.21 ± 0.05 (SEM) of the distance of the two electrodes. Thus, the optical measurement has a linear spatial resolution about 5 times better than the electrode measurement and a two-dimensional resolution about 25 times better.

Confocal and two-photon microscopes. The confocal microscope (Petran and Hadravsky, 1966) substantially reduces both the scattered and out-of-focus light that contributes to the image. A recent modification using two-photon excitation of the fluorophore further reduces out-of-focus fluorescence and photobleaching (Denk *et al.,* 1995). The spatial resolution of images from intact vertebrate preparations is much better with these types of microscope than with ordinary microscopy. These microscopes have been successfully used to monitor changes in calcium concentration inside small processes of neurons (Eilers *et al.,* 1995; Yuste and Denk, 1995). However, at present the sensitivity of these microscopes is relatively poor and they are relatively slow; there are no reports of their use to measure the small signals obtained with voltage-sensitive dyes of the type discussed in this article. On the other hand, slower voltage-sensitive dye signals have been measured confocally (Loew, 1993).

Random-access fluorescence microscopy. Bullen *et al.* (1997) have used acousto-optic deflectors to construct a random-scanning microscope and were able to measure signals from parts of cultured hippocampal neurons. To reduce the effects of fluctuations in the laser output, the fluorescence signals were divided by the output of a photodetector sampling the incident light. Relatively large

signal-to-noise ratios were obtained using voltage-sensitive dyes. This method has the advantage that only a small proportion of the preparation is illuminated, thereby reducing photodynamic damage from the very bright laser light source. However, this method will probably be restricted to preparations such as cultured neurons, in which there is relatively little light scattering.

Photodetectors. Because the signal-to-noise ratio in a shot-noise–limited measurement is proportional to the square root of the number of photons converted into photoelectrons (see above), quantum efficiency is important. Silicon photodiodes have quantum efficiencies approaching the ideal (1.0) at wavelengths at which most dyes absorb or emit light (500–900 nm). In contrast, only specially chosen vacuum photocathode devices (phototubes, photomultipliers, or image intensifiers) have a quantum efficiency as high as 0.15. Thus, in shot-noise–limited situations, a silicon diode has a signal-to-noise ratio that is at least 2.5 times larger. Photographic film has an even smaller quantum efficiency (0.01; Shaw, 1979), and thus has not been used for the kinds of measurements discussed in this paper.

Imaging devices. Many factors must be considered in choosing an imaging system. Perhaps the most important are the requirements for spatial and temporal resolution. Because the signal-to-noise ratio in a shot-noise–limited measurement is proportional to the number of measured photons, increases in either temporal or spatial resolution reduce the signal-to-noise ratio. Our discussion considers systems that have frame rates near 1 kHz. In most of these systems, the camera has been placed in the objective image plane of a microscope. However, Tank and Ahmed (1985) suggested a scheme by which a hexagonal close-packed array of optical fibers is positioned in the image plane, and individual photodiodes are connected to the other end of the optical fibers. NeuroPlex, a 464-pixel photodiode array camera (RedShirtImaging, LLC, Fairfield, CT) is based on this scheme.

Silicon diode arrays.

1. Parallel readout arrays. Diode arrays with from 124 to 1020 elements are now used in several laboratories (*e.g.,* Iijima *et al.,* 1989; Zecevic *et al.,* 1989; Nakashima *et al.,* 1992; Hirota *et al.,* 1995). In addition, Hammamatsu has constructed a system with 2500 elements. These arrays are designed for parallel readout; each detector is followed by its own amplifier, whose output can be digitized at frame rates of 1 kHz. Although the need to provide a separate amplifier for each diode element limits the number of pixels in parallel read-out systems, it contributes to the very large (10^5) dynamic range that these systems can achieve. Amplifiers have been discussed by Wu and Cohen (1993). Two parallel readout array systems are commercially available: Argus-50 (256 pix-

Table 1

Characteristics of fast CCD camera systems (as reported by the manufacturer)

Camera system	Frame rate (HZ) full frame	Well size (×1000 e)	Read noise (electrons)	Back illum.	Bits a-to-d	Pixels
BrainVision[1]	1600				12	92 × 64
Dalsa CA-D1-0128[2]	756				12	128 × 128
LSR, NeuroCAM UltraPix[3]	500	300	5 @100 Hz	yes	12	80 × 80
RedShirtImaging NeuroCCD[4]	2700	200	35 @1000 Hz	yes	14	74 × 74
TILL Photonics, IMAGO[5]	140	35	14 @140 Hz	no	12	160 × 120

A blank space indicates that the data were not available. The World Wide Web sites listed below were accessed on 15 November 1999.

[1] www.brainVision.co.jp

[2] www.dalsa.com

[3] www.lsr.co.uk/cameras/ultragraph.htm

[4] www.redshirtimaging.com

[5] www.till-photonics.com

els), manufactured by Hammamatsu Photonics K.K. (www.hpk.co.jp), and NeuroPlex (464 pixels), by RedShirtImaging, LLC (www.redshirtimaging.com).

2. Serial readout arrays. Use of a serial readout greatly reduces the number of amplifiers. In addition, it is simple to cool CCD (charge-coupled device) chips to reduce the dark noise. However, because of saturation, presently available CCD cameras are not optimal for the higher intensities available in some neurobiological experiments (Fig. 11). The high-intensity limit of the CCD camera is set by the light intensity that fills the electron wells on the CCD chip. This accounts for the bending over of the CCD camera performance at segment B in Figure 11. A dynamic range of even 10^3 is not easily achieved with a CCD camera. A CCD camera will not be optimal for measurements of absorption or for fluorescence measurements on *in vitro* slices and intact brains in measurements where all of the membranes are stained (Fig. 11). The light intensity would have to be reduced, with a consequent decrease in signal-to-noise ratio. On the other hand, CCD cameras are close to ideal for measurements from individual neurons stained with internally injected dyes. Table 1 compares several CCD cameras with frame rates near 1 kHz.

3. Vacuum photocathode cameras. Although the lower quantum efficiencies of vacuum photocathodes are a disadvantage, these devices may have lower dark noise. One such device, a Radechon (Kazan and Knoll, 1968), has an output proportional to the changes in the input. Vacuum photocathode cameras have been used in relatively low time resolution recordings from mammalian cortex (Blasdel and Salama, 1986) and salamander olfactory bulb (Kauer, 1988; Cinelli *et al.,* 1995) and are used in the Imager 2001, Optical Imaging, Inc. (www.opt-imaging.com).

Future Directions

Improvements in Sensitivity

Because the apparatus for measuring light is already reasonably optimized (see above), large improvements in the sensitivity of the techniques that use voltage-sensitive dyes must come from the development of better dyes or from investigating signals from other optical properties of the dyes. The dyes in Figure 9 and most of those synthesized are of the general class named polyenes (Hamer, 1964), a group that was first used to extend the wavelength response of photographic film. It is possible that improvements in signal size can be obtained with new polyene dyes (see Waggoner and Grinvald, 1977, and Fromherz *et al.,* 1991, for a discussion of maximum possible fractional changes in absorption and fluorescence). On the other hand, the fractional change on squid axons has not increased in recent years (Gupta *et al.,* 1981; L. B. Cohen, A. Grinvald, K. Kamino, and B. M. Salzberg, unpub. data), and most improvements (*e.g.,* Grinvald *et al.,* 1982b; Momose-Sato *et al.,* 1995; Tsau *et al.,* 1996; Antic and Zecevic, 1995) have involved synthesizing analogs that work well on new preparations.

The best of the styryl and oxonol polyene dyes have fluorescence changes of 10%–20%/100 mV when the staining is specific to the membrane whose potential is changing (Grinvald *et al.,* 1982b; Loew *et al.,* 1992; Rohr and Salzberg, 1994). Recently, Gonzalez and Tsien (1995) introduced a new scheme for generating voltage-sensitive signals using two chromophores and energy transfer. Although these fractional changes were also in the range of 10%/100 mV, more recent results are about 30% (J. Gonzalez and R. Tsien, pers. comm.). However, because one of the chromophores must be very hydrophobic and does not penetrate into brain tissue, it has not been possible to measure signals with this pair of dyes in intact tissues (T. Gonzalez and R. Tsien, A. Obaid and B. M. Salzberg; pers. comm.).

Bouevitch *et al.* (1993) and Ben-Oren *et al.* (1996) found that membrane potential changed the generation of nonlinear second harmonics from styryl dyes in cholesterol bilayers and in fly eyes. Large (50%) fractional changes were measured. It is hoped that improvements in the illumination intensity will result in larger signal-to-noise ratios.

Ehrenberg and Berezin (1984) have used resonance Raman to study surface potential; these methods might also be applicable for measuring transmembrane potential.

Improvements in Selectivity

An important new direction is the development of methods for neuron-type–specific staining. Three quite different approaches have been tried. First, the use of retrograde staining has been investigated in the embryonic chick and lamprey spinal cords (Tsau *et al.,* 1996). An identified cell class (motoneurons) was selectively stained. In lamprey experiments, spike signals from individual neurons were sometimes measured (Hickie *et al.,* 1996). Further efforts to optimize this staining procedure are needed. Second is the use of cell-type–specific staining developed for fluorescein by Nirenberg and Cepko (1993). It might be possible to use similar techniques to selectively stain cells with voltage-sensitive or ion-sensitive dyes. Third, Siegel and Isacoff (1997) constructed a genetically encoded combination of a potassium channel and green fluorescent protein. When introduced into a frog oocyte, this molecule had a (relatively slow) voltage-dependent signal with a fractional fluorescence change of 5%. Neuron-type–specific staining would make it possible to determine the role of specific neuron types in generating the input-output function of a brain region.

Optical recordings already provide unique insights into brain activity and organization. Improvements in sensitivity or selectivity would make these methods more powerful.

Acknowledgments

Literature Cited

Adrian, E. D. 1942. Olfactory reactions in the brain of the hedgehog. *J. Physiol.* **100:** 459–473.

Albowitz, B., and U. Kuhnt. 1993. Spread of epileptiform potentials in the neocortical slice: recordings with voltage-sensitive dyes. *Brain Res.* **631:** 329–333.

Antic, S., and D. Zecevic. 1995. Optical signals from neurons with internally applied voltage-sensitive dyes. *J. Neurosci.* **15:** 1392–1405.

Antic, S., G. Major, and D. Zecevic. 1999. Fast optical recording of membrane potential changes from dendrites of pyramidal neurons. *J. Neurophysiol.* **82:** 1615–1621.

Ben-Oren, I., G. Peleg, A. Lewis, B. Minke, and L. Loew. 1996. Infrared nonlinear optical measurements of membrane potential in photoreceptor cells. *Biophys. J.* **71:** 1616–1620.

Beuerman, R. W. 1975. Slow potentials of the turtle olfactory bulb in response to odor stimulation of the nose. *Brain Res.* **97(1):** 61–78.

Blasdel, G. G., and G. Salama. 1986. Voltage-sensitive dyes reveal a modular organization in monkey striate cortex. *Nature* **321:** 579–585.

Bouevitch, O., A. Lewis, I. Pinevsky, J. Wuskell, and L. Loew. 1993. Probing membrane potential with nonlinear optics. *Biophys. J.* **65:** 672–679.

Boyle, M. B., and L. B. Cohen. 1980. Birefringence signals that monitor membrane potential in cell bodies of molluscan neurons. *Fed. Proc.* **39:** 2130.

Braddick, H. J. J. 1960. Photoelectric photometry. *Rep. Prog. Physics* **23:** 154–175.

Bullen, A., S. S. Patel, and P. Saggau. 1997. High-speed, random-access fluorescence microscopy: I. High resolution optical recording with voltage-sensitive dyes and ion indicators. *Biophys. J.* **73:** 477–491.

Bullock, T. H., and M. C. McClune. 1989. Lateral coherence of the electrocorticogram: a new measure of brain synchrony. *Electroencephalogr. Clin. Neurophysiol.* **73:** 479–498.

Cinelli, A. R., and B. M. Salzberg. 1992. Dendritic origin of late events in optical recordings from salamander olfactory bulb. *J. Neurophysiol.* **68:** 786–806.

Cinelli, A. R., S. R. Neff, and J. S. Kauer. 1995. Salamander olfactory bulb neuronal activity observed by video rate, voltage-sensitive dye imaging. I. Characterization of the recording system. *J. Neurophysiol.* **73:** 2017–2032.

Cohen, L. B., and S. Lesher. 1986. Optical monitoring of membrane potential: methods of multisite optical measurement. *Soc. Gen. Physiol. Ser.* **40:** 71–99.

Cohen, L. B., and B. M. Salzberg. 1978. Optical measurement of membrane potential. *Rev. Physiol. Biochem. Pharmacol.* **83:** 35–88.

Dainty, J. C. 1984. *Laser Speckle and Related Phenomena.* Springer-Verlag, New York.

Davila, H. V., B. M. Salzberg, L. B. Cohen, and A. S. Waggoner. 1973. A large change in axon fluorescence that provides a promising method for measuring membrane potential. *Nat. New. Biol.* **241:** 159–160.

Davila, H. V., L. B. Cohen, B. M. Salzberg, and B. B. Shrivastav. 1974. Changes in ANS and TNS fluorescence in giant axons from *Loligo. J. Membr. Biol.* **15:** 29–46.

Delaney, K. R., A. Gelperin, M. S. Fee, J. A. Flores, R. Gervais, D. W. Tank, and D. Kleinfeld. 1994. Waves and stimulus-modulated dynamics in an oscillating olfactory network. *Proc. Nat. Acad. Sci.* **91:** 669–673.

Denk, W., D. W. Piston, and W. Webb. 1995. Two-photon molecular excitation in laser-scanning microscopy. Pp. 445–458 in *Handbook of Biological Confocal Microscopy,* J. W. Pawley ed. Plenum Press, New York.

Ehrenberg, B., and Y. Berezin. 1984. Surface potential on purple membranes and its sidedness studied by resonance Raman dye probe. *Biophys. J.* **45:** 663–670.

Eilers, J., G. Callewaert, C. Armstrong, and A. Konnerth. 1995. Calcium signaling in a narrow somatic submembrane shell during synaptic activity in cerebellar Purkinje neurons. *Proc. Nat. Acad. Sci. US* **92:** 10272–10276.

Freeman, W. J. 1978. Spatial Properties of an EEG Event in the Olfactory Bulb and Cortex. *Electroencephalogr. Clin. Neurophysiol.* **44:** 586–605.

Fromherz, P., K. H. Dambacher, H. Ephardt, A. Lambacher, C. O.

Muller, R. Neigl, H. Schaden, O. Schenk, and T. Vetter. 1991. Fluorescent dyes as probes of voltage transients in neuron membranes: progress report. *Ber. Bunsen-Ges. Phys. Chem.* **95:** 1333–1345.

Gonzalez, J. E., and R. Y. Tsien. 1995. Voltage sensing by fluorescence resonance energy transfer in single cells. *Biophys. J.* **69:** 1272–1280.

Grinvald, A., A. Manker, and M. Segal. 1982a. Visualization of the spread of electrical activity in rat hippocampal slices by voltage-sensitive optical probes. *J. Physiol. (Lond)* **333:** 269–291.

Grinvald, A., R. Hildesheim, I. C. Farber, and L. Anglister. 1982b. Improved fluorescent probes for the measurement of rapid changes in membrane potential. *Biophys. J.* **39:** 301–308.

Grinvald, A., B. M. Salzberg, V. Lev-Ram, and R. Hildesheim. 1987. Optical recording of synaptic potentials from processes of single neurons using intracellular potentiometric dyes. *Biophys. J.* **51:** 643–651.

Grinvald, A., R. D. Frostig, E. Lieke, and R. Hildesheim. 1988. Optical imaging of neuronal activity. *Physiol. Rev.* **68:** 1285–1366.

Gross, E., R. S. Bedlack Jr., and L. M. Loew. 1994. Dual-wavelength ratiometric fluorescence measurements of the membrane dipole potential. *Biophys. J.* **67:** 208–216.

Gupta, R. K., B. M. Salzberg, A. Grinvald, L. B. Cohen, K. Kamino, S. Lesher, M. B. Boyle, A. S. Waggoner, and C. H. Wang. 1981. Improvements in optical methods for measuring rapid changes in membrane potential. *J. Membr. Biol.* **58:** 123–137.

Hamer, F. M. 1964. *The Cyanine Dyes and Related Compounds.* Wiley, New York.

Hickie, C., P. Wenner, M. O'Donovan, Y. Tsau, J. Fang, and L. B. Cohen. 1996. Optical monitoring of activity from individual and identified populations of neurons retrogradely labeled with voltage-sensitive dyes. *Soc. Neurosci. Abstr.* **22:** 321.

Hirota, A., K. Sato, Y. Momose-Sato, T. Sakai, and K. Kamino. 1995. A new simultaneous 1020-site optical recording system for monitoring neural activity using voltage-sensitive dyes. *J. Neurosci. Methods* **56:** 187–194.

Hughes, J. R., and J. A. Mazurowski. 1962. Studies on the supracallosal mesial cortex of unanesthetized, conscious mammals. II Monkey. B. Responses from the olfactory bulb. *Electroencephalogr. Clin. Neurophysiol.* **14:** 635–645.

Iijima, T., M. Ichikawa, and G. Matsumoto. 1989. Optical monitoring of LTP and related phenomena. *Soc. Neurosci. Abstr.* **15:** 398.

Inoué, S. 1986. *Video Microscopy.* Plenum Press, New York. p 128.

Kauer, J. S. 1988. Real-time imaging of evoked activity in local circuits of the salamander olfactory bulb. *Nature* **331:** 166–168.

Kazan, B., and M. Knoll. 1968. *Electronic Image Storage.* Academic Press, New York.

Kleinfeld, D., and K. R. Delaney. 1996. Distributed representation of vibrissa movement in the upper layers of somatosensory cortex revealed with voltage-sensitive dyes. *J. Comp. Neurol.* **375:** 89–108.

Kogan, A., W. N. Ross, D. Zecevic, and N. Lasser-Ross. 1995. Optical recording from cerebellar Purkinje cells using intracellularly injected voltage-sensitive dyes. *Brain Res.* **700:** 235–239.

Kupfermann, I., H. Pinsker, V. Castellucci, and E. R. Kandel. 1971. Central and peripheral control of gill movements in *Aplysia. Science* **174:** 1252–1256.

Lam, Y.-w., Lawrence B. Cohen, Matt Wachowiak, and Michal R. Zochowski. 2000. Odors elicit three different oscillations in the turtle olfactory bulb. *J. Neurosci.* In press.

Laurent, G., and M. Naraghi. 1994. Odorant-induced oscillations in the mushroom bodies of the locust. *J. Neurosci.* **14(5 Pt 2):** 2993–3004.

Loew, L. M. 1993. Confocal microscopy of potentiometric fluorescent dyes. *Methods Cell Biol.* **38:** 195–209.

Loew, L. M., L. B. Cohen, B. M. Salzberg, A. L. Obaid, and F. Bezanilla. 1985. Charge-shift probes of membrane potential. Characterization of aminostyrylpyridinium dyes on the squid giant axon. *Biophys. J.* **47:** 71–77.

Loew, L. M., L. B. Cohen, J. Dix, E. N. Fluhler, V. Montana, G. Salama, and J. Y. Wu. 1992. A napthyl analog of the aminostyryl pyridinium class of potentiometric membrane dyes shows consistent sensitivity in a variety of tissue, cell, and model membrane preparations. *J. Memb. Biol.* **130:** 1–10.

London, J. A., D. Zecevic, and L. B. Cohen. 1987. Simultaneous optical recording of activity from many neurons during feeding in *Navanax. J. Neurosci.* **7:** 649–661.

Magee, J. C., and D. Johnston. 1995. Synaptic activation of voltage-gated channels in the dendrites of hippocampal pyramidal neurons. *Science* **268:** 301–304.

Magee, J. C., G. Christofi, H. Miyakawa, B. Christie, N. Lasser-Ross, and D. Johnston. 1995. Subthreshold synaptic activation of voltage-gated calcium channels mediate a localized calcium influx into dendrites of hippocampal pyramidal neurons. *J. Neurophysiol.* **74:** 335–342.

Mainen, Z. F., N. T. Carnevalle, A. M. Zador, B. J. Claiborne, and T. H. Brown. 1996. Electronic architecture of hippocampal CA1 pyramidal neurons based on three-dimensional reconstructions. *J. Neurophysiol.* **76:** 1904–1923.

Malmstadt, H. V., C. G. Enke, S. R. Crouch, and G. Harlick. 1974. *Electronic Measurements for Scientists.* Benjamin, Menlo Park, CA.

Markram, H., and B. Sakmann. 1994. Calcium transients in dendrites of neocortical neurons evoked by single subthreshold excitatory postsynaptic potentials *via* low-voltage-activated calcium channels. *Proc. Nat. Acad. Sci.* **91:** 5207–5211.

Momose-Sato, Y., K. Sato, T. Sakai, A. Hirota, K. Matsutani, and K. Kamino. 1995. Evaluation of optimal voltage-sensitive dyes for optical measurement of embryonic neural activity. *J. Membr. Biol.* **144:** 167–176.

Nakashima, M., S. Yamada, S. Shiono, M. Maeda, and F. Satoh. 1992. 448-detector optical recording system: development and application to *Aplysia* gill-withdrawal reflex. *IEEE Trans. Biomed. Eng.* **39:** 26–36.

Nirenberg, S., and C. Cepko. 1993. Targeted ablation of diverse cell classes in the nervous system *in vivo. J. Neurosci.* **13:** 3238–3251.

Obaid, A. L., T. Koyano, J. Lindstrom, T. Sakai, and B. M. Salzberg. 1999. Spatiotemporal patterns of activity in an intact mammalian network with single-cell resolution: optical studies of nicotinic activity in an enteric plexus. *J. Neurosci.* **19:** 3073–3093.

Orbach, H. S., and L. B. Cohen. 1983. Optical monitoring of activity from many areas of the *in vitro* and *in vivo* salamander olfactory bulb: a new method for studying functional organization in the vertebrate central nervous system. *J. Neurosci.* **3:** 2251–2262.

Orbach, H. S., L. B. Cohen, and A. Grinvald. 1985. Optical mapping of electrical activity in rat somatosensory and visual cortex. *J. Neurosci.* **5:** 1886–1895.

Petran, M., and M. Hadravsky. 1966. Czechoslovakian patent 7720.

Prechtl, J. C., L. B. Cohen, B. Peseran, P. P. Mitra, and D. Kleinfeld. 1997. Visual stimuli induce waves of electrical activity in turtle cortex. *Proc. Nat. Acad. Sci. USA* **94:** 7621–7626.

Ratzlaff, E. H., and A. Grinvald. 1991. A tandem-lens epifluorescence microscope: hundred-fold brightness advantage for wide-field imaging. *J. Neurosci. Meth.* **36:** 127–137.

Rohr, S., and B. M. Salzberg. 1994. Multiple site optical recording of transmembrane voltage in patterned growth heart cell cultures: assessing electrical behavior, with microsecond resolution, on a cellular and subcellular scale. *Biophys. J.* **67:** 1301–1315.

Ross, W. N., and L. F. Reichardt. 1979. Species-specific effects on the optical signals of voltage-sensitive dyes. *J. Membr. Biol.* **48:** 343–356.

Ross, W. N., B. M. Salzberg, L. B. Cohen, A. Grinvald, H. V. Davila, A. S. Waggoner, and C. H. Wang. 1977. Changes in absorption, fluorescence, dichroism, and birefringence in stained giant axons: optical measurement of membrane potential. *J. Membr. Biol.* **33:** 141–183.

Sakai, T., A. Hirota, H. Komuro, S. Fujii, and K. Kamino. 1985. Optical recording of membrane potential responses from early embryonic chick ganglia using voltage-sensitive dyes. *Brain Res.* **349:** 39–51.

Salama, G. 1988. Voltage-sensitive dyes and imaging techniques reveal new patterns of electrical activity in heart and cortex. *Proc. SPIE (Int. Soc. Optical Eng.)* **94:** 75–86.

Salzberg, B. M. 1983. Optical recording of electrical activity in neurons using molecular probes. Pp. 139–187 in *Current Methods in Cellular Neurobiology.* J. L. Barker and J. F. McKelvy, eds. Wiley, New York.

Salzberg, B. M., H. V. Davila, and L. B. Cohen. 1973. Optical recording of impulses in individual neurones of an invertebrate central nervous system. *Nature* **246:** 508–509.

Salzberg, B. M., A. Grinvald, L. B. Cohen, H. V. Davila, and W. N. Ross. 1977. Optical recording of neuronal activity in an invertebrate central nervous system: simultaneous monitoring of several neurons. *J. Neurophysiol.* **40:** 1281–1291.

Schiller, J., F. Helmchen, and B. Sakmann. 1995. Spatial profile of dendritic calcium transients evoked by action potentials in rat neocortical pyramidal neurons. *J. Physiol.* **487:** 583–600.

Shaw, R. 1979. Photographic detectors. *Appl. Optics Optical Eng.* **7:** 121–154.

Siegel, M. S., and E. Y. Isacoff. 1997. A genetically encoded optical probe of membrane voltage. *Neuron* **19:** 735–41.

Spruston, N., Y. Schiller, G. Stuart, and B. Sakmann. 1995. Activity-dependent action potential invasion and calcium influx into hippocampal CA1 dendrites. *Science* **268:** 297–300.

Stuart, G. J., and B. Sakmann. 1994. Active propagation of somatic action potentials into neocortical pyramidal cell dendrites. *Nature* **367:** 69–72.

Tank, D., and Z. Ahmed. 1985. Multiple-site monitoring of activity in cultured neurons. *Biophys. J.* **47:** 476A.

Tsau, Y., J. Y. Wu, H. P. Hopp, L. B. Cohen, D. Schiminovich, and C. X. Falk. 1994. Distributed aspects of the response to siphon touch in *Aplysia:* spread of stimulus information and cross-correlation analysis. *J. Neurosci.* **14:** 4167–4184.

Tsau, Y., P. Wenner, M. J. O'Donovan, L. B. Cohen, L. M. Loew, and J. P. Wuskell. 1996. Dye screening and signal-to-noise ratio for retrogradely transported voltage-sensitive dyes. *J. Neurosci. Meth.* **70:** 121–129.

Waggoner, A. S. 1979. Dye indicators of membrane potential. *Annu. Rev. Biophys. Bioeng.* **8:** 47–68.

Waggoner, A. S., and A. Grinvald. 1977. Mechanisms of rapid optical changes of potential sensitive dyes. *Annu. NY Acad. Sci.* **303:** 217–241.

Wu, J. Y., and L. B. Cohen. 1993. Fast multisite optical measurements of membrane potential. Pp. 389–404 in *Fluorescent and Luminescent Probes for Biological Activity.* W. T. Mason, ed. Academic Press, London.

Wu, J. Y., L. B. Cohen, and C. X. Falk. 1994a. Neuronal activity during different behaviors suggests a distributed neuronal organization in the *Aplysia* abdominal ganglion. *Science* **263:** 820–823.

Wu, J. Y., Y. Tsau, H. P. Hopp, L. B. Cohen, A. C. Tang, and C. X. Falk. 1994b. Consistency in nervous systems: trial-to-trial and animal-to-animal variations in the response to repeated application of a sensory stimulus in *Aplysia. J. Neurosci.* **14:** 1366–1384.

Wu, J. Y., Y. W. Lam, C. X. Falk, L. B. Cohen, J. Fang, L. Loew, J. C. Prechtl, D. Kleinfeld, and Y. Tsau. 1998. Voltage-sensitive dyes for monitoring multi-neuronal activity in the intact CNS. *Histochem. J.* **30:** 169–187.

Yuste, R., and W. Denk. 1995. Dendritic spines as basic functional units of neuronal integration. *Nature* **375:** 682–684.

Zecevic, D. 1996. Multiple spike-initiation zones in single neurons revealed by voltage-sensitive dyes. *Nature* **381:** 322–325.

Zecevic, D., J. Y. Wu, L. B. Cohen, J. A. London, H. P. Hopp, and C. X. Falk. 1989. Hundreds of neurons in the *Aplysia* abdominal ganglion are active during the gill-withdrawal reflex. *J. Neurosci.* **9:** 3681–3689.